Master's Thesis

3D printed supporter combined with dopamine coated hydrogel-based carbon for highly efficient and self-floating solar steam generator

Se-Young Kang

Department of Energy Engineering

(Energy Engineering)

Graduate School of UNIST

2019

3D printed supporter combined with dopamine coated hydrogel-based carbon for highly efficient and self-floating solar steam generator

Se-Young Kang

Department of Energy Engineering
(Energy Engineering)

Graduate School of UNIST

3D printed supporter combined with dopamine coated hydrogel-based carbon for highly efficient and self-floating solar steam generator

A thesis/dissertation
submitted to the Graduate School of UNIST
in partial fulfillment of the
requirements for the degree of
Master of Science

Se-Young Kang

06. 15. 2019
Approved by

_____

Advisor
Ji-Hyun Jang

3D printed supporter combined with dopamine coated hydrogel-based carbon for highly efficient and self-floating solar steam generator

Se-Young Kang

This certifies that the thesis/dissertation of Se-Young Kang is approved.

06. 15. 2019

signature

_____

Advisor: Ji-Hyun Jang

signature

_____

typed name: Jongnam Park

signature

_____

typed name: Jin Young Kim

Abstract

Research on solar desalination especially can make easily and portable device, which is called solar still has been researched in various ways. Also, the 3D printer has already been commercialized in various fields. In this study, we developed a supporter that created in a simple way by using the 3D printer which is categorized in the DLP method, not only helps self-floating but also assists the steam generation by capillary force. Without any materials, this supporter can achieve a high mass change of ~1.083 kg/m^2h under one sun illumination. As a photo-absorber, we developed microporous material, hydrogel-based carbon (HBC), which has outstanding solar absorption of 98% between 250-2500 nm, is produced by the CVD method. In addition, the HBC's hydrophobic property can prevent salt rejection that makes good stability in the solar desalination process which can extremely increase the sustainable performance. Finally, polydopamine coating treatment applies to commercial GF/C membrane to achieve surface immobilization, combined with HBC by the vacuum filtration process. This solar still device is a combination of HBC on the top layer, polydopamine coated GF/C membrane located at beneath it, and 3D printed supported on the bottom. It exhibits average evaporation rates of ~1.728kg/m^2h with an excellent solar conversion efficiency of up to 89% under 1 sun illumination also shows high performance in terms of sustainability. With its unique hydrophobic porous black material (HBC) assembled with self-floating 3d printed supporter is an efficient and sustainable solar vapor generator which can also serve as high-salinity brine desalination.

Contents

Abstract **5**
List of Figures **7**
I. Introduction **9**
1.1 Review of solar desalination **9**
1.2 Review of Solar still **12**
1.3 References **14**

2. Experimental section of 3D printed supporter combined with dopamine coated hydrogel-based carbon for highly efficient and self-floating solar steam generator **15**
2.1 Experimental section **15**
2.1.1 Chemicals **15**
2.1.2 Fabrication of hydrogel-based carbon **15**
2.1.3 Synthesis of reduced Graphene Oxide **15**
2.1.4 Preparation of pDA coated GF/C membrane **15**
2.2 Results and discussion **16**
2.2.1 Build 3D printed supporter **16**
2.2.2 Fabrication of 3D-SGD **18**
2.2.3 Characterization **21**
2.2.3.1 3D printed supporter **21**
2.2.3.2 pDA coated GF/C membrane **22**
2.2.3.3 Hydrogel based carbon (HBC) **29**
2.2.4 Photothermal performance **33**
2.2.4.1 Enhanced performance by 3D printed supporter **33**
2.2.4.2 Enhanced performance by pDA coated GF/C membrane **39**
2.2.4.3 Enhanced performance by HBC **44**
2.2.4.4 Mass change and conversion efficiency by HBC **49**
2.3 Conclusion **51**
2.4 References **52**

List of Figures

Figure 1.1. Global water demand gap between 2010 and 2030 10

Figure 1.2. Annual new contracted desalination capacities by feed water, 1990-2010 10

Figure 1.3. Classification according to the process of solar thermal desalination. We conducted research on solar 11

Figure 1.4. Standard shape of solar still device 12

Figure 1.5. Key factors to consider when creating a solar still device 13

Figure 2.1. Schematic of making 3D printed supporter to assign self-floating property 16

Figure 2.2. Digital camera image of the 3D printed we used. This 3D printer is NYOMO's 'MINNY' which is the categorized by DLP method 3D printer. 17

Figure 2.3. Drawing of 3D printed self-floating supporter. The air pocket is designed as shown in the figure 19

Figure 2.4. Schematic of how to develop 3D printed solar steam generation device (3D-SGD) 20

Figure 2.5. Schematic of how to develop 3D printed solar steam generation device (3D-SGD 21

Figure 2.6. Digital camera images of changes in GF/C membrane by time when it dips into polydopamine solution 22

Figure 2.7. SEM images of changes in GF/C membrane by time when it dips into polydopamine solution 23

Figure 2.8. FTIR spectra of GF/C, 2DRS-D4, 2DRS-D8, 2DRS-D12, 2DRS-D24 showing the chemical composition 25

Figure 2.9. XPS spectra of GF/C, 2DRS-D4, 2DRS-D8, 2DRS-D12, 2DRS-D24 showing the atomic composition ratio 26

Figure 2.10. XPS spectra of GF/C, 2DRS-D4, 2DRS-D8, 2DRS-D12, 2DRS-D24 that separate by C1s, O1s, N1s peak 27

Figure 2.11. Atomic weight percentage of GF/C, 2DRS-D4, 2DRS-D8, 2DRS-D12, 2DRS-D24 collected by XPS 28

Figure 2.12. XPS characterization of 25 different polydopamine-coated surfaces. The bar graph represents the intensity of characteristic substrate signal before (hatched) and after (solid) coating by polydopamine 28

Figure 2.13. SEM images of HBC. Various types of pores ranging from nanometer to micrometer size detected 30

Figure 2.14. BET investigation of the surface area and the pore size distribution of (a) HBC, (b) rGO, (c) Graphite, (d) SWCNT 31

Figure 2.15. Magnified absorption graph for (a) HBC, (b)rGO, (c) Graphite, (d) SWCNT from 300nm to 2500nm wavelength 32

Figure 2.16. 3D printed supporter based on the difference between surface curvature and z-axis value of plane, 20RS, 20DRS, 40DRS. This illustration shows how the light is reflected at the

surface of the samples when it receives light 34
Figure 2.17. Diffuse reflectance of plane, 20RS, 20DRS, and 40DRS 35
Figure 2.18. Measured thermal conductivity differences by thermal imaging camera (FL-IR)..... 36
Figure 2.19. Surface temperature and bulk water temperature change by time. 20DRS shows the highest surface temperature and at the same time it acts as a excellent insulator that effectively prevents the heat transfer to bulk water..... 37
Figure 2.20. Graph showing the water evaporation rate at 1sun for samples with flat surface and curved samples, further divided by the degree of curvature and z-axis value 38
Figure 2.21. Absorbance of pristine GF/C, 2DRS-D4, 2DRS-D8, 2DRS-D12, and 2DRS-D24. Increase dipping time give the better absorbance by itself..... 40
Figure 2.22. Graph shows the difference in absorbance when the HBC is raised on pristine GF/C and when it is on 2DRS-D24 41
Figure 2.23. Difference in adhesion confirmed by digital camera image. (a), (b) the back of the membranes, (c), (d) images that rubbed the front side of the membrane with HBC, (e), (f) images of each membrane immersed in water 42
Figure 2.24. The values of storage and loss modulus measured with dma with and without PDA coating treatment 43
Figure 2.25. Time dependent contact angles of hydrophobic membrane surfaces..... 45
Figure 2.26. (a) Mass change measured for 24 hours. (b) Cycle retention for 20 times 46
Figure 2.27. Zeta potential of HBC with various black materials (Graphite, rGO, and SWCNT) 47
Figure 2.28. Schematic of 3D-SGD for zeta potential aspect. High negative zeta potential lead to high osmotic pressure that promote absorption of water from bulk water to top..... 48
Figure 2.29. Real-time seawater weight loss through the evaporation of the 3D-SGD with different polydopamine dipping time 50

I. Introduction

1.1 Solar desalination

The need for clean water is a serious threat to the development of human civilization. No matter how advanced society is, it is necessary to improve the quality of life of all human beings. According to the United Nations report, about 1.2 billion people, or about one-fifth of the world's population live in water-scarce areas, and another 500 million people are expected to suffer shortages of water in near future. In addition, about 1.6 billion people, or one-quarter of the world's population faces water shortages for economic reasons. Figure 1.1 shows that global water demand gap between 2010 and 2030. Water that can be eaten without going through the desalination process on the earth continues to decrease, but the demand for water is expected to increase by about 53% by 2030. Therefore, desalination can be a powerful tool to overcome the increasing demand for water. In terms of the types of water to be desalinated or purified, desalination of seawater, which occupies a large part of the earth, is being studied extensively. Figure 1.2 shows that seawater desalination has experienced major market expansion since 2003.

The dramatic increase of desalinated water supply would create a series of problems, the most significant of which are those related to energy consumption and environmental pollution caused by the using of fossil fuels. It is estimated that 8.78 million tons of oil per year is needed to produce 1 million m^3/day fresh water. It is very important to find suitable alternative energy sources for desalination systems. For this reason, the need for energy that is environmentally friendly, abundant and does not create side effects such as global warming has become inevitable. The most suitable energy for these conditions was sunlight, so research on solar thermal desalination has been actively conducted. Desalination can be achieved by using many techniques. Desalination techniques classified by two types.

(i) phase-change or thermal processes; and

(ii) membrane or single-phase processes.

Also, it is classified simply in figure 1.3. We have experimented with solar still, which is a direct process of various solar desalination techniques.

.

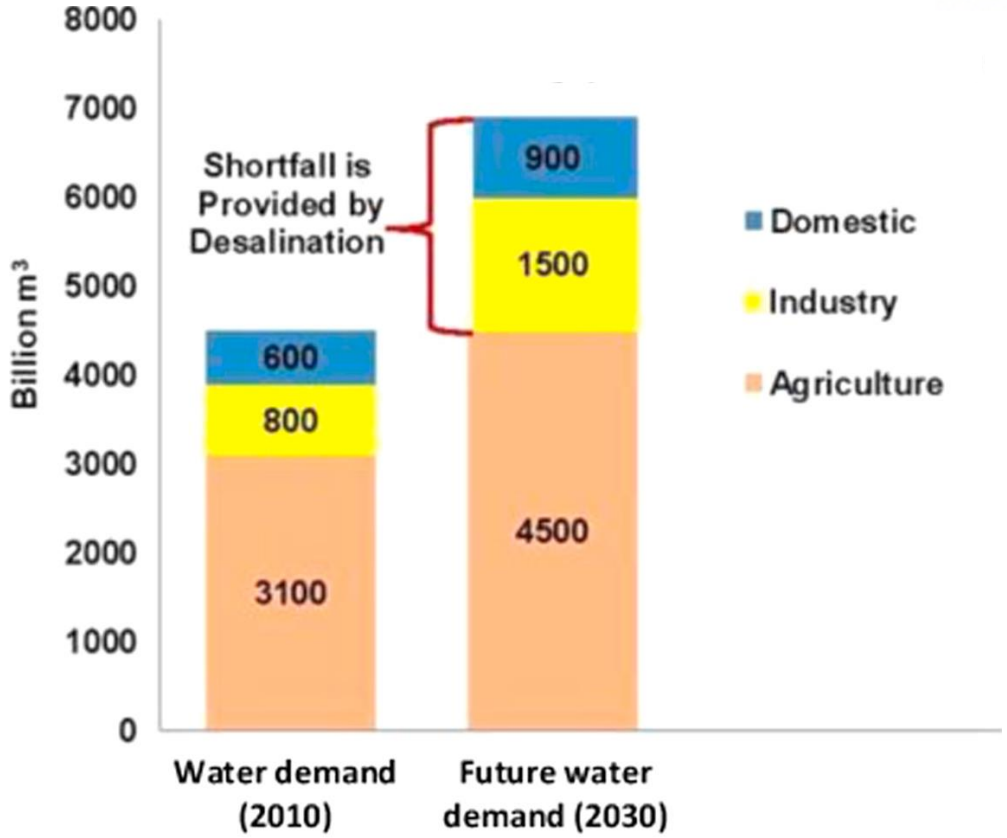

Figure 1.1 Global water demand gap between 2010 and 2030.

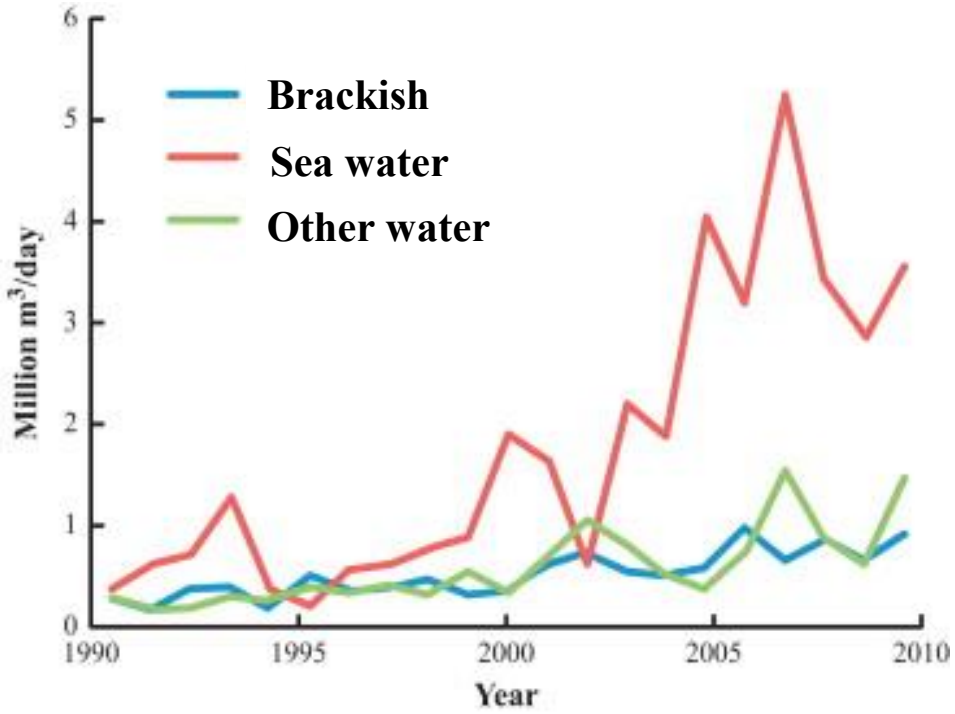

Figure 1.2 Annual new contracted desalination capacities by feed water, 1990-2010.

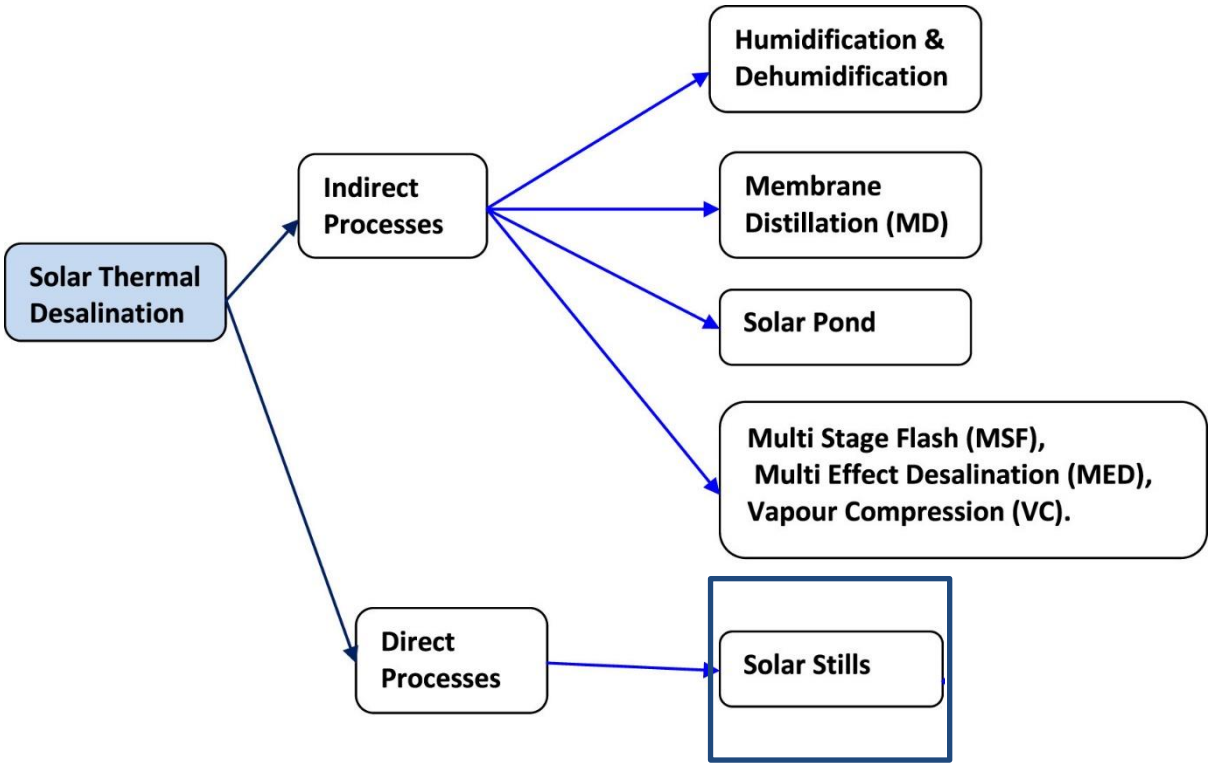

Figure 1.3 Classification according to the process of solar thermal desalination. We conducted research on solar.

1.2 Solar still

At its lowest cost per liter, solar still is elliptical sunlight, a single branch that is still coupled to a vacuum tube collector and is a cascading solar cell with external and internal reflectors. The solar still has a black basin full of brine or brine and is covered with sloped glass that fills to a certain depth and promotes the transfer of solar radiation and condensation. Figure 1.4 shows the standard shape of the solar still device. The solar radiation coming into the basin heats the black liner and heats the water causing evaporation. Due to the difference in partial pressure and the temperature difference, the water vapor condenses along with the tilted glass cover and is collected under appropriate conditions on the floor.

There are three major factors that affect the performance of the solar still. The first is environmental factors, which we cannot control, whether we can get a lot of sunlight, get enough temperature, proper humidity and wind. The second is the design of the device. How much area the light can receive, how deep the water is, how much condensation the material used, and how effectively the heat transfer to the bulk water can be prevented, etc. In the field of a solar still, creating a design that meets these qualities is a big challenge. The last is how solar desalination operates. It can be also easily controlled. How much dust such as salt accumulates on the surface, how well the water is pulled up, and the position of the solar still. This is well documented in figure 1.5. We have successfully developed solar still device by considered second and third of the main factors and experimented with the goal of developing solar still with high efficiency and good sustainability.

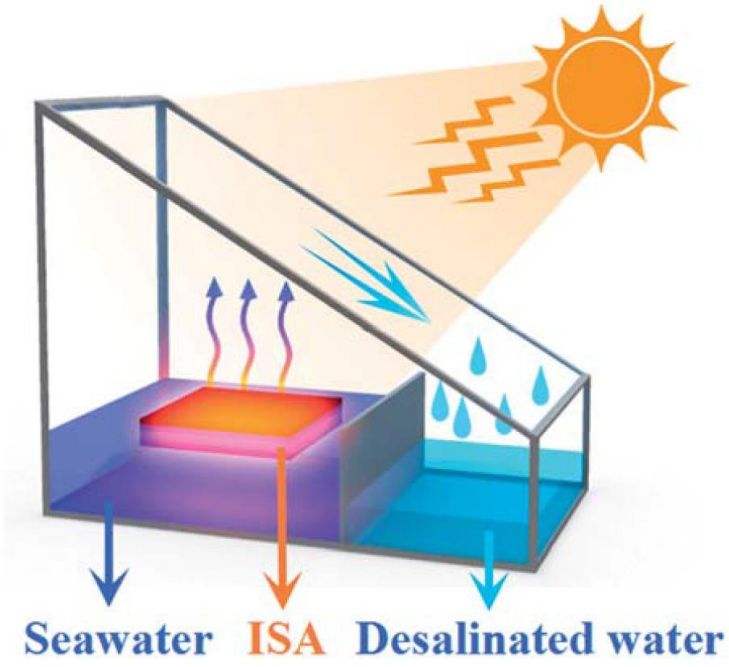

Figure 1.4 Standard shape of solar still device.

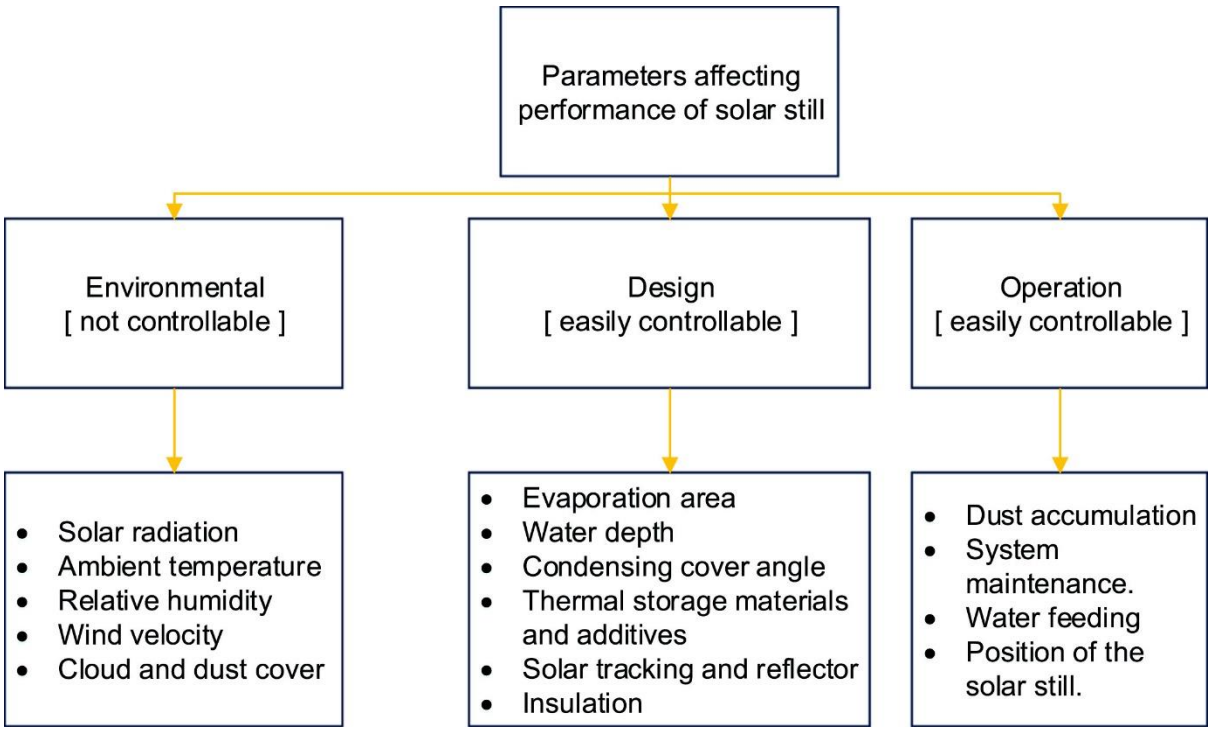

Figure 1.5 Key factors to consider when creating a solar still device.

1.4 References

[1] H.Sharon, and K.S.Reddy, “A review of solar energy driven desalination technologies”, Renewable and Sustainable Energy Reviews, 2015, 41, 1080-1118.

[2] Chennan Li, Yogi Goswami, and Elias Stefanakos, “Solar assisted sea water desalination: A review”, Renewable and Sustainable Energy Reviews, 2013, 19, 136-163.

[3] M.Khayet, “Solar desalination by membrane distillation: Dispersion in energy consumption analysis and water production costs (a review)”, Desalination, 2013, 308, 89-101.

[4] Gang Xiao, Xihui Wang, Mingjiang Ni, Fei Wang, Weijun Zhu, Zhongyang Luo, and Kefa Cen “A review on solar stills for brine desalination”, Applied Energy, 2013, 103, 642-652

[5 Lourdes García-Rodríguez, “Seawater desalination driven by renewable energies: a review”, Desalination, 2002, 143, 103-113.

2.1 Experimental Section

2.1.1 Chemicals

Chemicals including PVA with an average molecular weight of 50000, PVP with an average molecular weight of 360000, GF/C membrane, dopamine hydrochloride, ethanol (99.8%), hydrochloric acid (37%) were purchased from sigma-Aldrich. graphite powder, potassium persulfate, sulfuric acid (98%) were also purchased from Sigma-Aldrich.

2.1.2 Fabrication of hydrogel-based carbon (HBC)

To fabricate the microporous carbon, the precursor was collected from supramolecular hydrogel by freeze-drying It was successively heated up to 300°C by 5°C/min, 500°C by 1°C./min, and 1000°C by 5°C/min. It was kept at a constant 1000°C for 1hour in Argon atmosphere. Obtained black materials are etched in 37 % HCl solution and washed by enough dilute water.

2.1.3 Synthesis of reduced Graphene Oxide

The graphene oxide was synthesized using the hummer's method. First, the mixture of flake graphite/$NaNO_3$ was prepared in 2:1 weight ratio. The mixture was added into a beaker with a certain amount of 98 wt.% H_2SO_4 and a suspension was obtained. Keep the condition using ice bath, slowly add 3g KMnO4, raise to 35°C using a hot water bath. Stir this mixture for 1 hour from when the temperature is reached to 35°C. The bright yellow resulted suspension was filtered by the qualitative filter paper when it was still hot, and the solid mixture was washed with dilute HCl aqueous and distilled water and dried in vacuum oven at 70°C for 24 h.

Hydrazine hydrate was added into suspension and heated at 80°C for 24 hours, and the weight ratio of hydrazine hydrate and GO was controlled at 10:7. A kind of black flocculent substance was gradually precipitated out of the solution. The product was obtained by filtered with the qualitative filter paper. Finally, the resulting black product was washed with water and dried at 80°C for 24 h.

2.1.4 Preparation of pDA coated GF/C membrane

Coating polydopamine to a commercial GF / C membrane process is briefly described in fig. 2.4. First, dissolve dopamine hydrochloride (10 mM) in Ethanol (99.8%). Piperidine (20 mM) is then added to the above solution to serve as an oxidizing agent and to aid in self-polymerization. The GF / C membrane was immersed in a dopamine solution for 4 hours, 8 hours, 12 hours, 24 hours, and 100 hours, and the change of mass change was compared.

2.2. Results and discussion

2.2.1 Build 3D printed supporter

The 3D printed supporter was designed by 3ds max (2018 ver.). To maximize the capillary force and maintain the highest resolution of the 3d printer, we used a triangle as the base grid of the pattern. To make a self-floating effect in the sample, we designed an air pocket on the edge of the supporter. However, even if air pockets were designed in the program, there was a case in which the empty space is not cured. Therefore, the printed sample didn't float on the water. To solve this problem, we designed a hole in six places on the edge (Fig. 2.1). By this way, the inside of the printed sample was sufficiently cured through the hole, also internal shape could sufficiently preserve. To make the sample for perfect drying, nitrogen blowing was performed. The resin was then applied to the hole and blocked with a UV lamp by curing. This procedure has prevented the inner collapse and finally made the sample self-floating by the inner air-pocket.

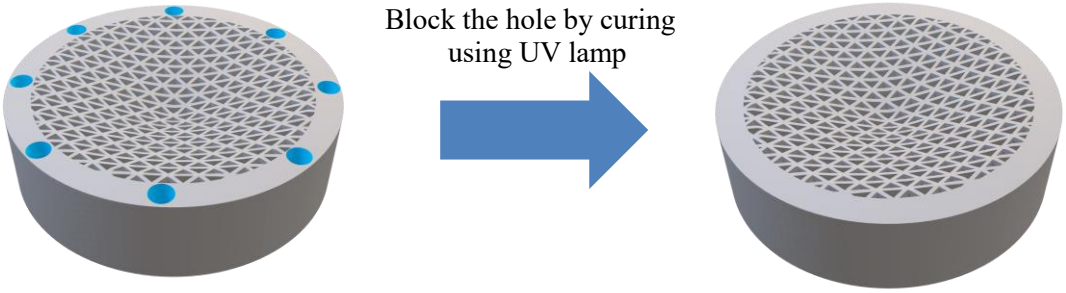

Figure 2.2. Schematic of making 3D printed supporter to assign self-floating property.

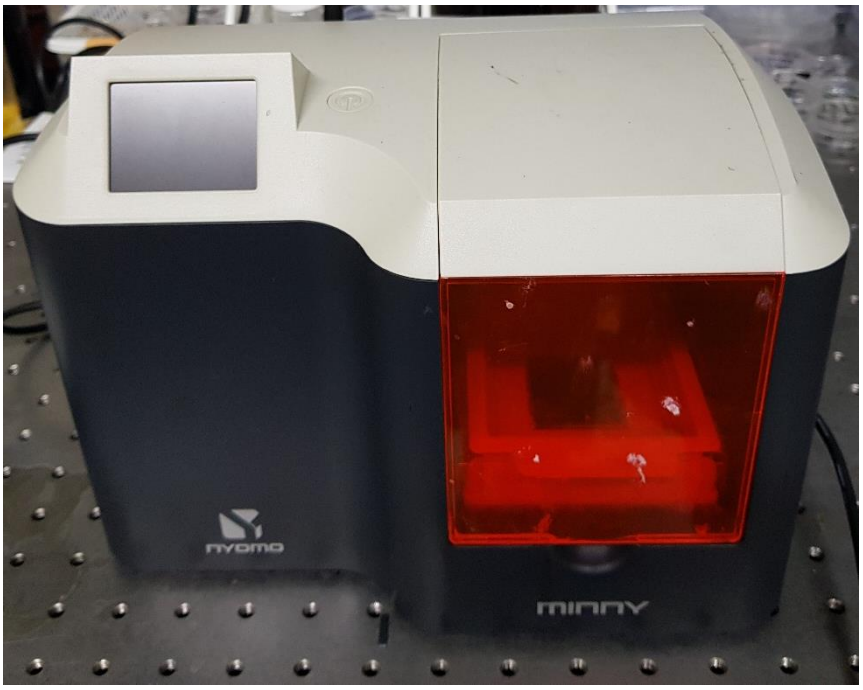

Figure 2.2. It is the actual image of the 3d printer used in the laboratory. This 3D printer is NYOMO's 'MINNY' which is the categorized by DLP method 3D printer.

2.2.2 Fabrication of 3D-SGD

The process of making the 3d printed solar steam generation device(3D-SGD) is illustrated in figure 2.4. commercial GF/C membrane was used to assist evaporation of water by its hydrophilicity and support to raise the black materials. This GF/C membrane was immersed in a dopamine solution and subjected to polydopamine coating treatment via the self-polymerization process. The conventional method has been used pH 8.5 tris buffer to make it similar with the seawater environment. But we used piperidine as an organic base which could help oxidizes the dopamine molecules in the pure organic solvents for the rapid formation of the polydopamine coating layer. Figure 2.4 shows the process of completing the steam generation device using the polydopamine-coated GF/C membrane and hydrogel-based carbon. Mix the hydrogel base carbon and water in a ratio of 50:1 and drop on the GF / C membrane which is sufficiently treat with polydopamine in vacuum filter condition. Finally, the GF / C membrane with hydrogel-based carbon and the 3D printed supporter are attached with the instant glue. At this time, the instant glue is applied to the edge of the air pocket, which does not affect to solar desalination performance.

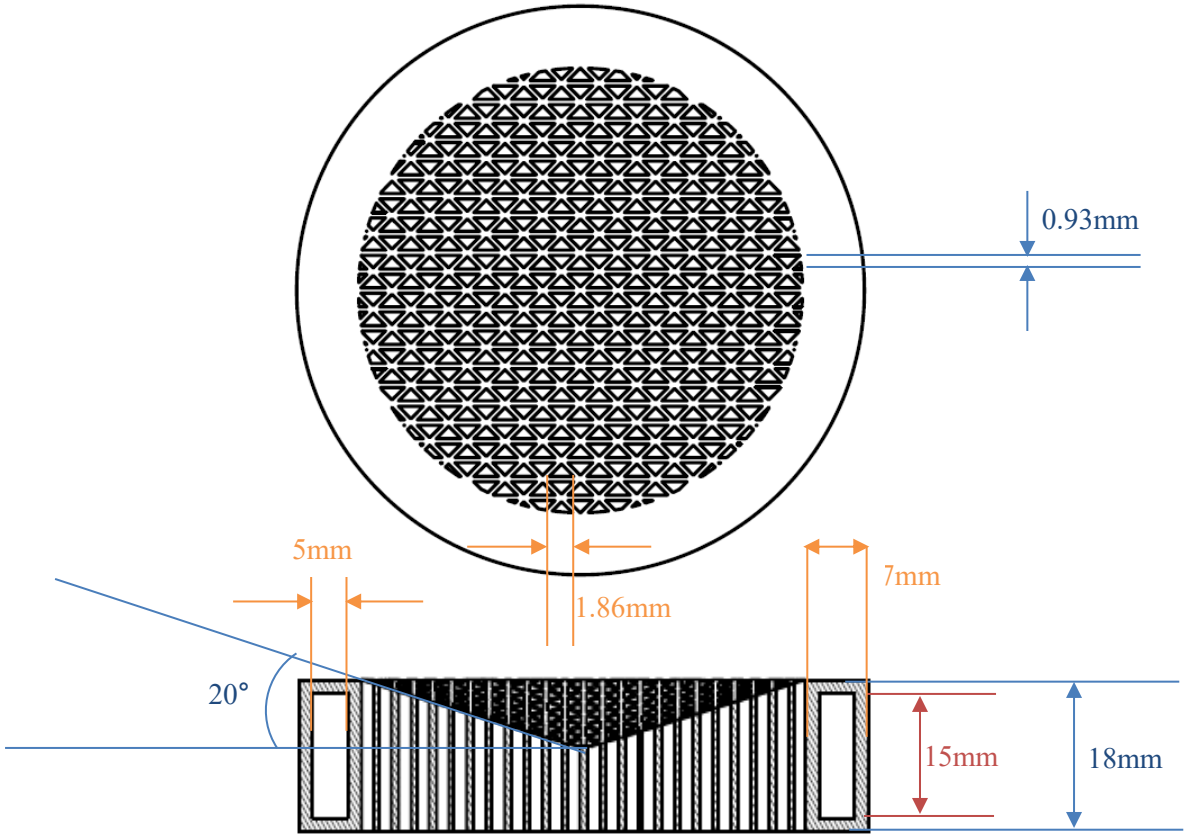

Figure 2.3. Drawing of 3D printed self-floating supporter. The air pocket is designed as shown in the figure.

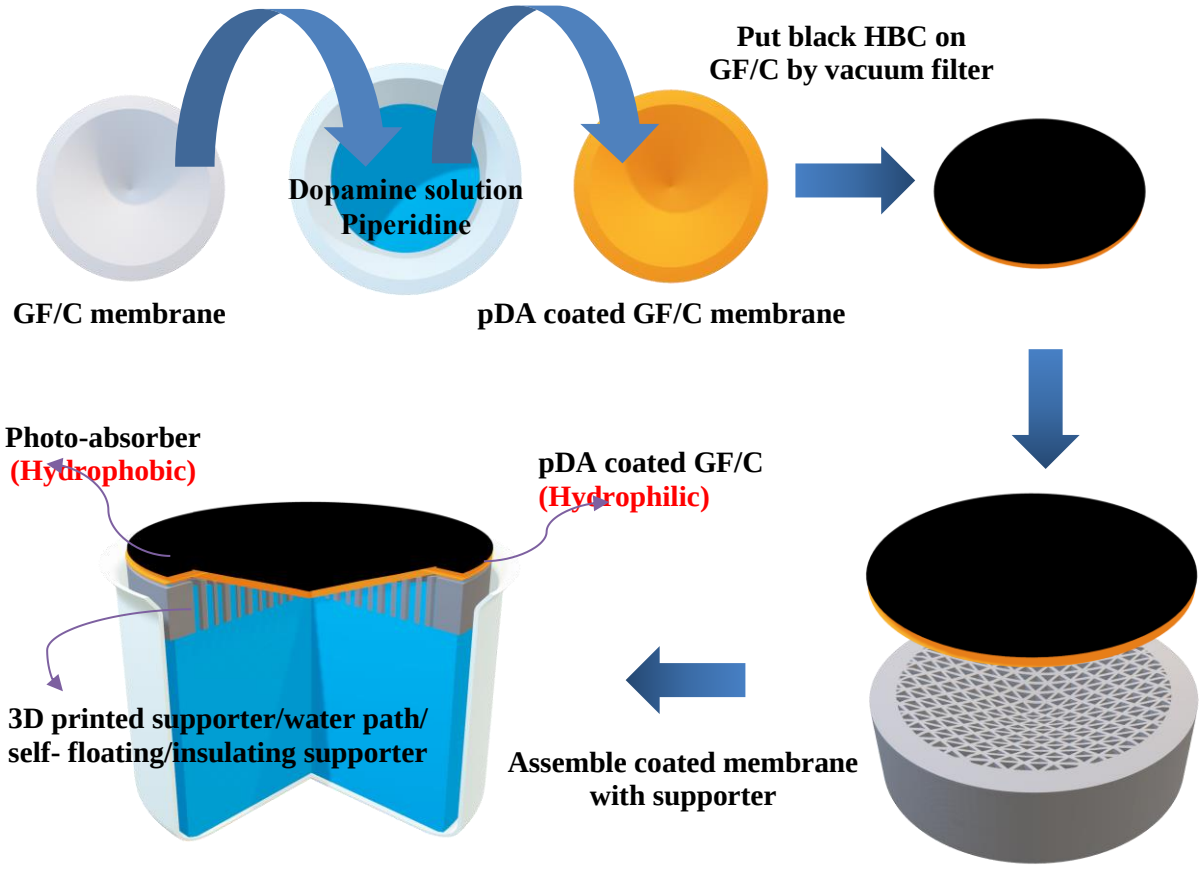

Figure 2.4. Schematic of how to develop 3D printed solar steam generation device(3D-SGD).

2.2.3 Characterization

2.2.3.1. 3D printed supporter

Figure 2.5 shows the digital camera image of 3D printed supporter and its Optical microscopy image. As shown in Figure 2.5(a), the uniform pattern is shown by setting the pattern grid length to the maximum resolution that can be drawn by a 3d printer. The inside of the edge has an air pocket, which is self-floating in the water. Figure 2.5(b)-(f) confirmed to be uniformly printed by microscopy and can play a role as a water path.

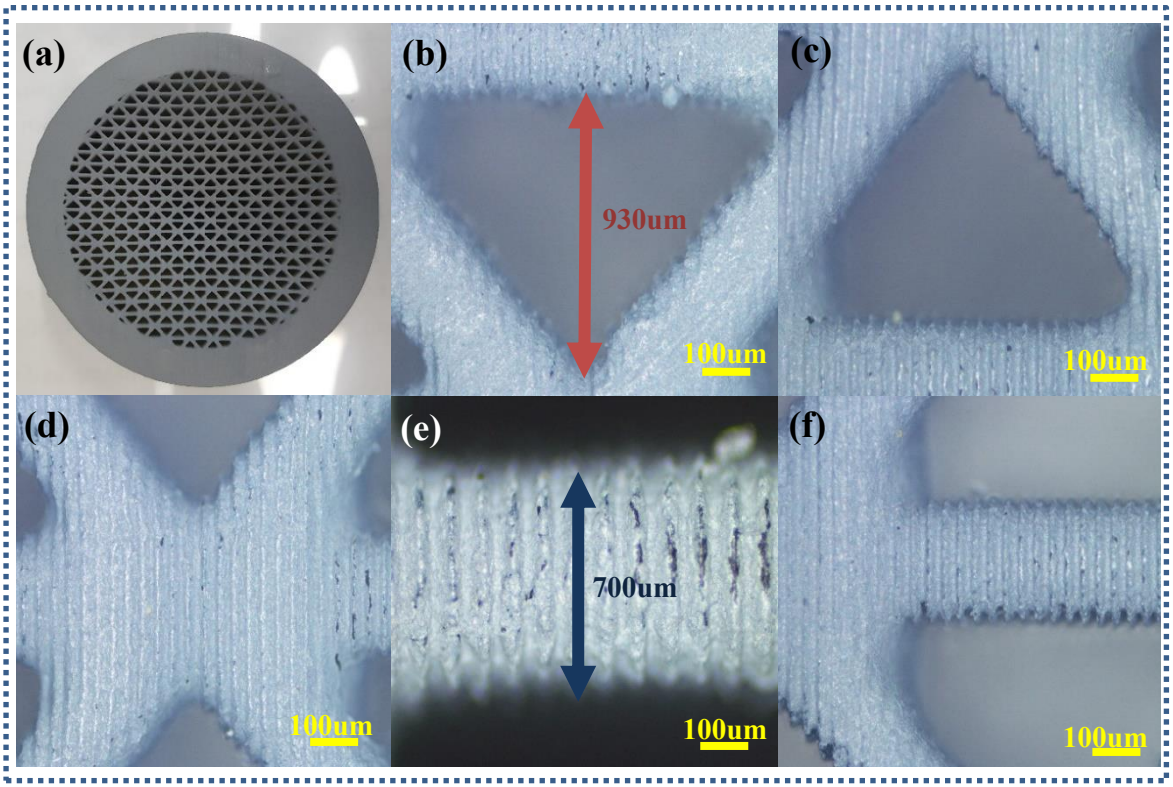

Figure 2.5. Schematic of how to develop 3D printed solar steam generation device(3D-SGD).

2.2.3.2. pDA coated GF/C membrane

Figure 2.6 shows the digital camera image taken after immersing the GF/C membrane in the dopamine solution over time. Increasing the dipping time by 4h, 8h, 12h, 24h yielded samples 2DRS-D4, 2DRS-D8, 2DRS-D12, 2DRS-D24, respectively, at fixed room temperature and dopamine solution's concentration. As you can see in these pictures, the longer the membrane is soaked, the more GF/C membrane becomes dark brown. Looking through the membrane by the SEM images (figure 2.7) the interpretation quite possible. Compared with pristine GF/C membranes, the longer the dipping time in the dopamine solution, the polydopamine molecules are wrapped around the fiber. The longer the membrane is immersed in the dopamine solution, the darker the color of the membrane and more dopamine is coated around the membrane fiber, as it will be seen in the data, it has a huge impact on mass change performance.

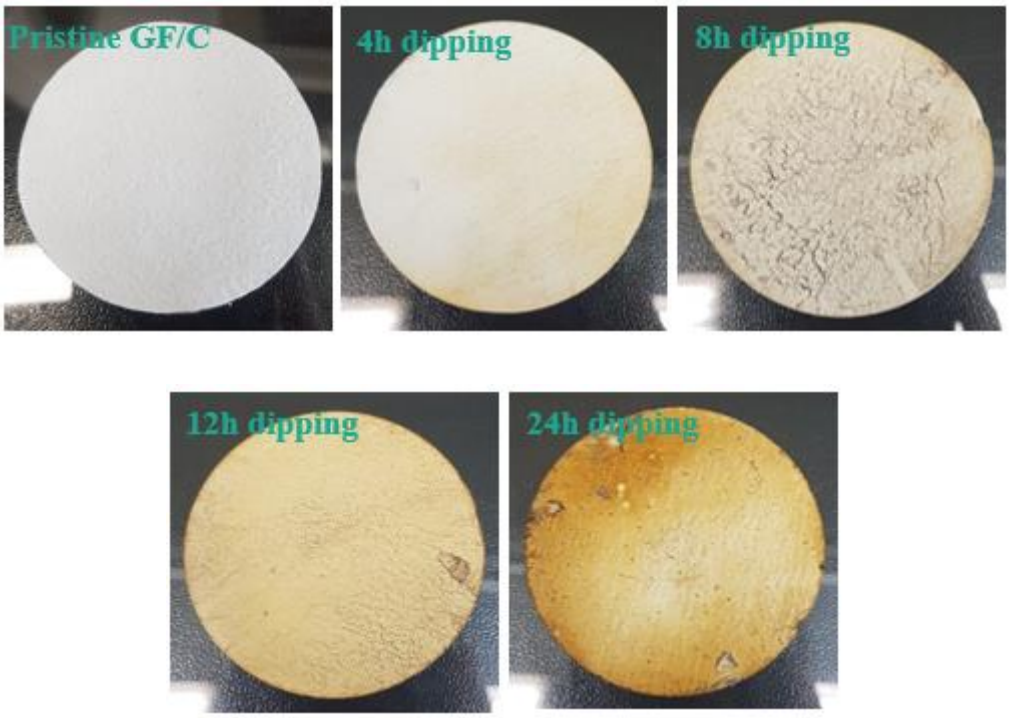

Figure 2.6. Digital camera images of changes in GF/C membrane by time when it dips into polydopamine solution.

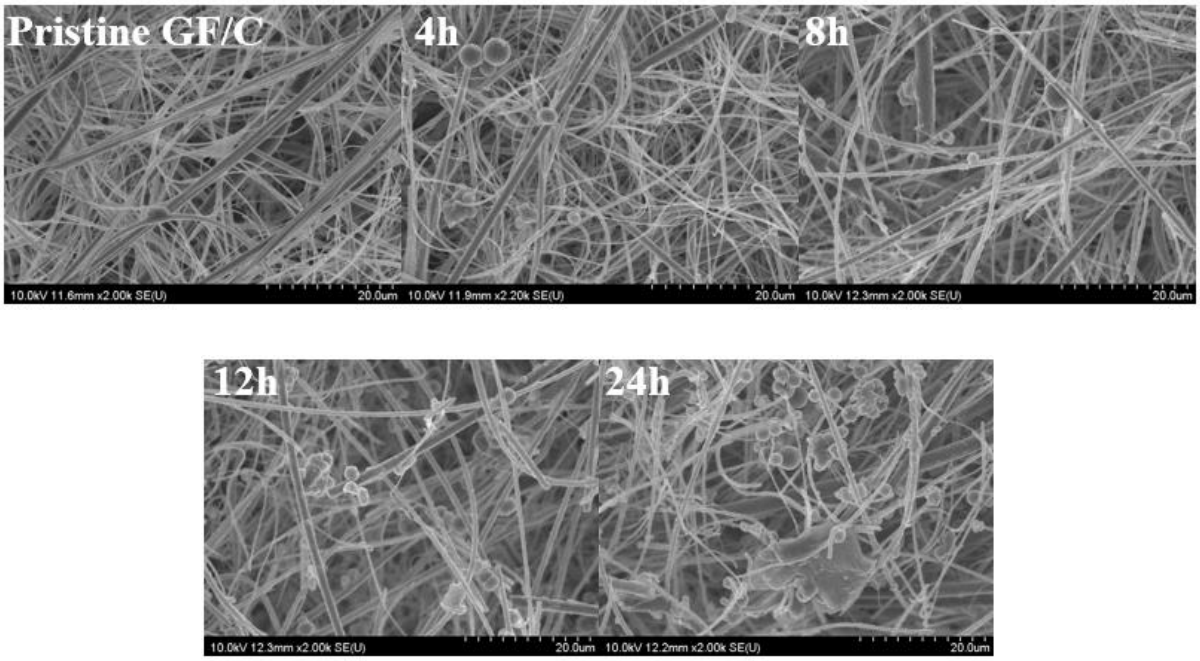

Figure 2.7. SEM images of changes in GF/C membrane by time when it dips into polydopamine solution.

Additional characterization of these samples was done with FT-IR, and XPS (Figure 2.8-10). FT-IR spectroscopy was performed to verify the surface chemical that checking how well the GF/C membrane was coated with polydopamine (Figure 2.8) Although 2DRS-D4 and 2DRS-D8 were dipped in the polydopamine solution for 4 hours and 8 hours, respectively, the IR picks did not differ significantly from the conventional GF/C membranes. However, upon dipping for 12 hours or more with PDA, some major bands were distinctly observed on the spectrum. A strong absorption band around 1613cm^{-1} arose from N-H(amide) vibrations. While peaks around 1512cm^{-1} were due to C=C, C=N stretching vibrations. Peaks at 1486cm^{-1} and 1268cm^{-1} were the characteristic absorption peaks of C-H(amide) and C-O(amide), respectively. Therefore, IR provides further evidence that dopamine has been polymerized onto GF/C membrane.

XPS was also used to investigate the atomic ratio of the pDA coated GF/C surfaces. As the dipping time increases, the atomic ratio of C1s gradually increases, the ratio of O1s gradually decreases, and the ratio of N1s gradually increases. Macroscopically, the content of N, which was rarely found in pristine GF/C membranes, was rapidly increased, indicating that dopamine was well coated on the membrane. In addition, the nitrogen-to carbon N/C atomic ratio is why the numbers for each ratio are important in this XPS data. N/C ratio of 2DRS-D12 and 2DRS-D24 were 0.130 and 0.129, respectively. It implied that the coating was derived from dopamine polymerization due to 0.125 is the theoretical N/C ratio for dopamine. Figure 2.11 is a graph showing the N/C ratio values when dopamine is successfully coated on various materials by self-polymerization. When the ratio value is placed between 0.1 and 0.13, it is reasonable to confirm that dopamine is well coated on the surfaces.

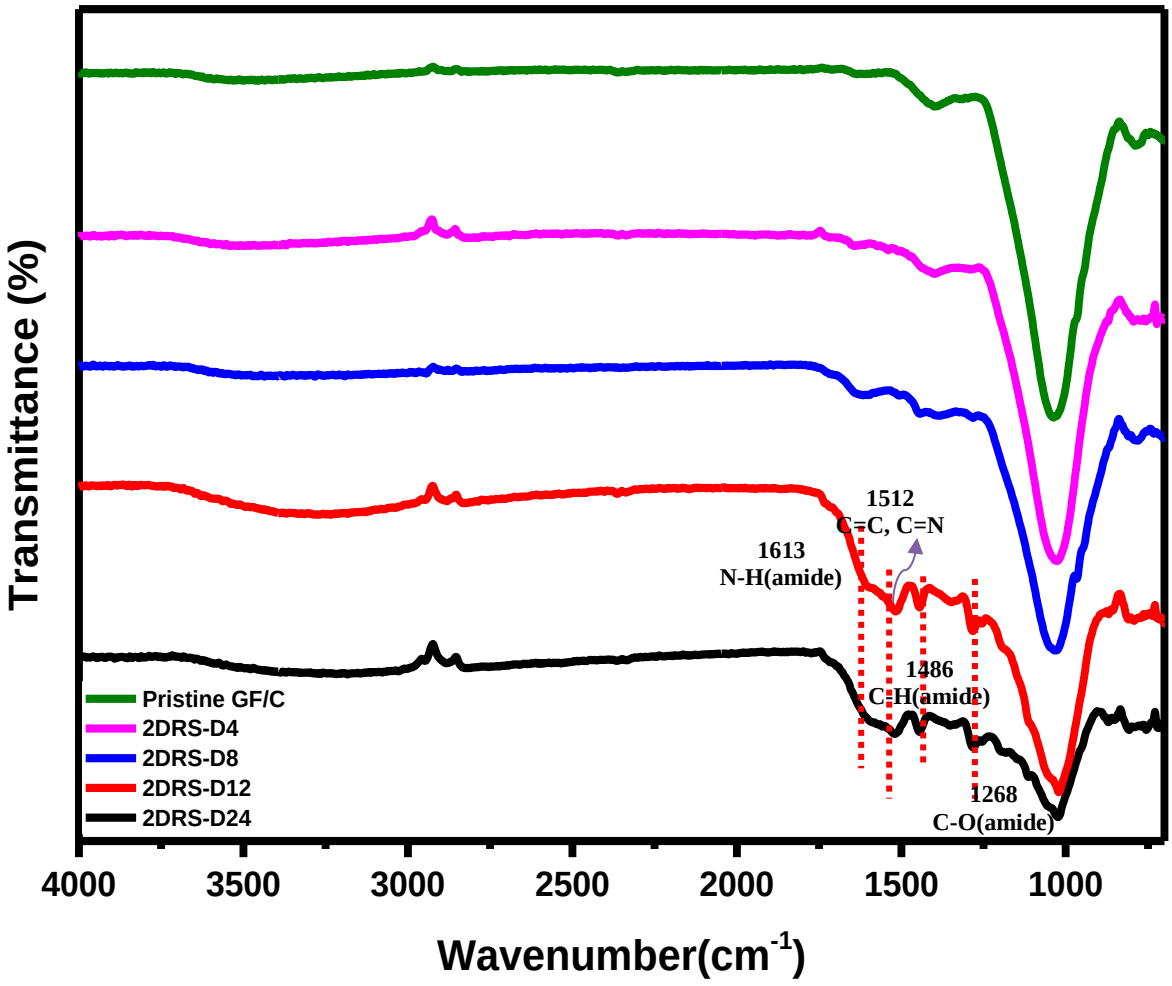

Figure 2.8. FTIR spectra of GF/C, 2DRS-D4, 2DRS-D8, 2DRS-D12, 2DRS-D24 showing the chemical composition.

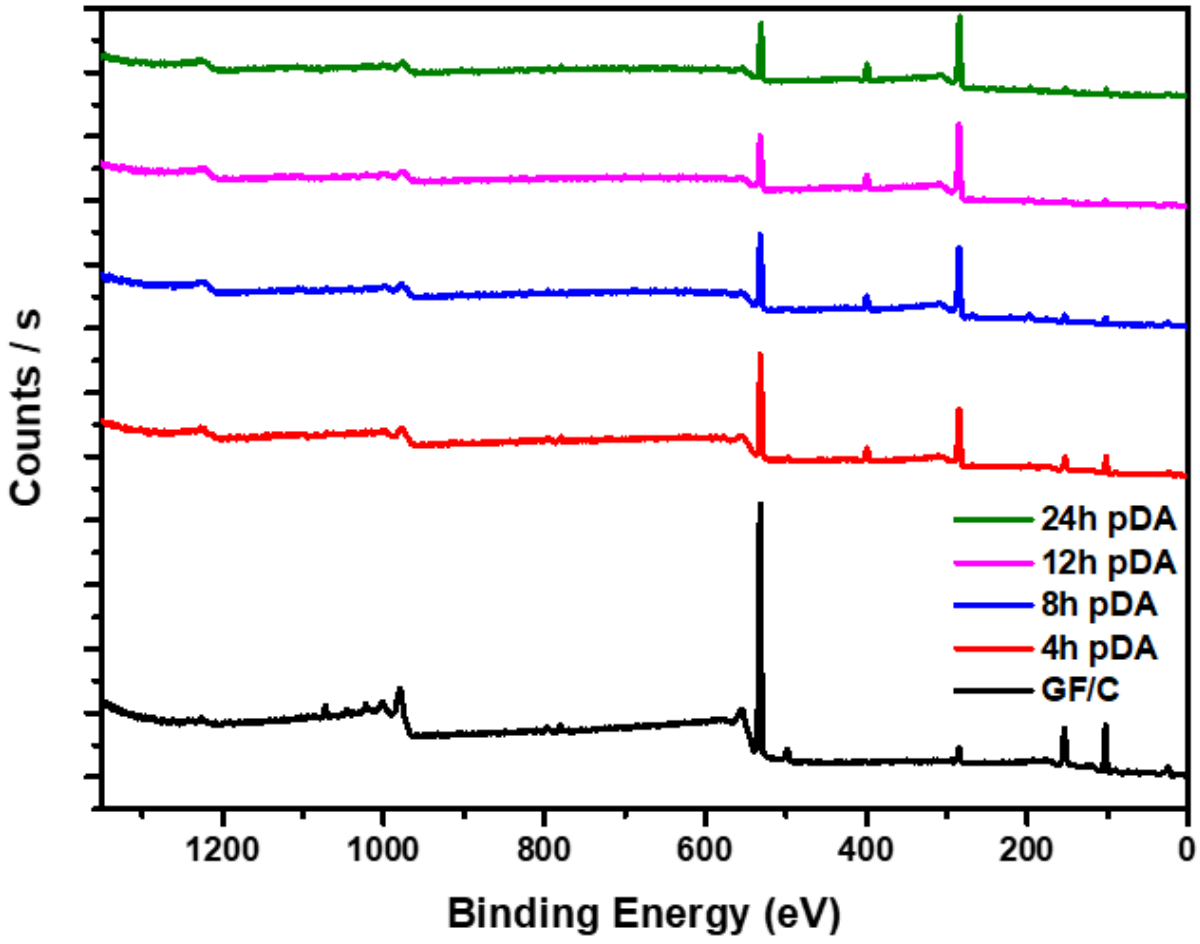

Figure 2.9. XPS spectra of GF/C, 2DRS-D4, 2DRS-D8, 2DRS-D12, 2DRS-D24 showing the atomic composition ratio.

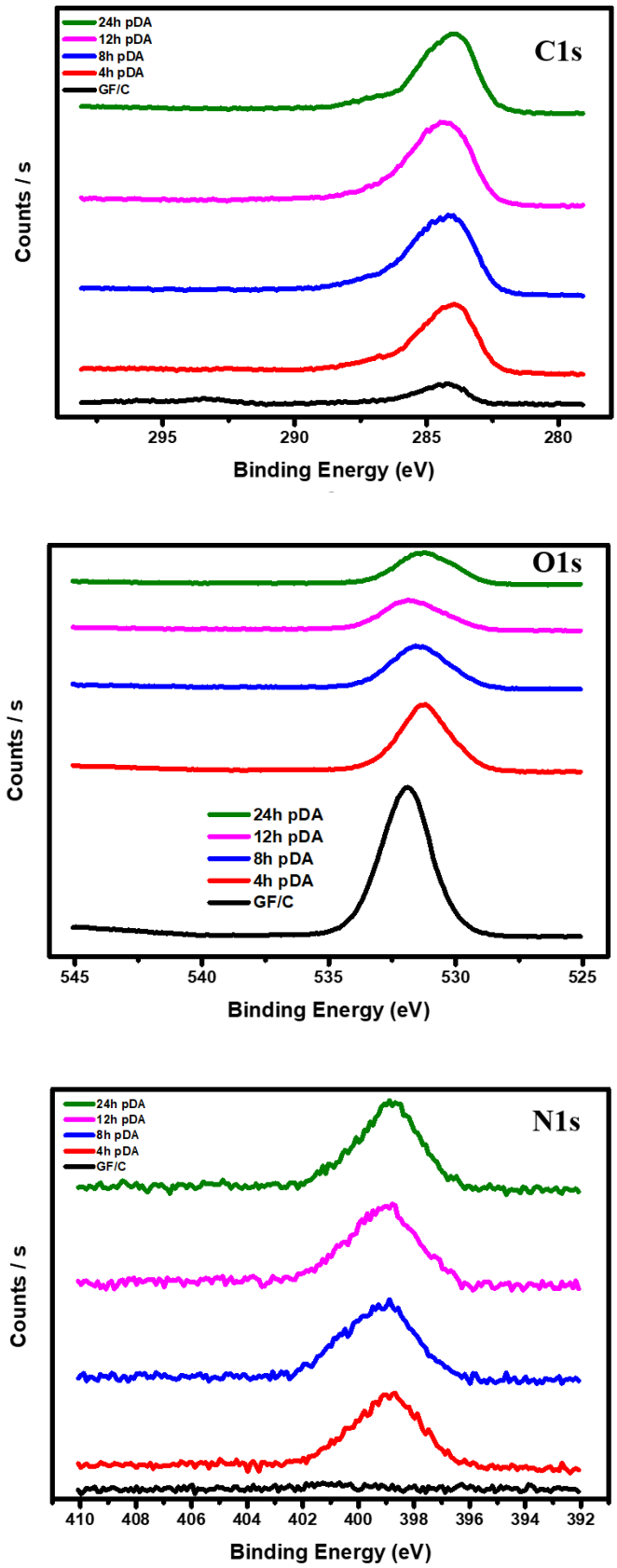

Figure 2.10. XPS spectra of GF/C, 2DRS-D4, 2DRS-D8, 2DRS-D12, 2DRS-D24 that separate by C1s, O1s, N1s peak.

	GF/C	4h	8h	12h	24h
	At. %	At. %	At. %	At. %	At. %
C1s	11.25	48.17	59.07	67.47	65.11
O1s	56.96	31.58	23.83	18.46	18.92
N1s	0.36	6.70	8.26	8.78	8.63
N/C ratio	0.032	0.139	0.140	0.130	0.129

Figure 2.11. Atomic weight percentage of GF/C, 2DRS-D4, 2DRS-D8, 2DRS-D12, 2DRS-D24 collected by XPS.

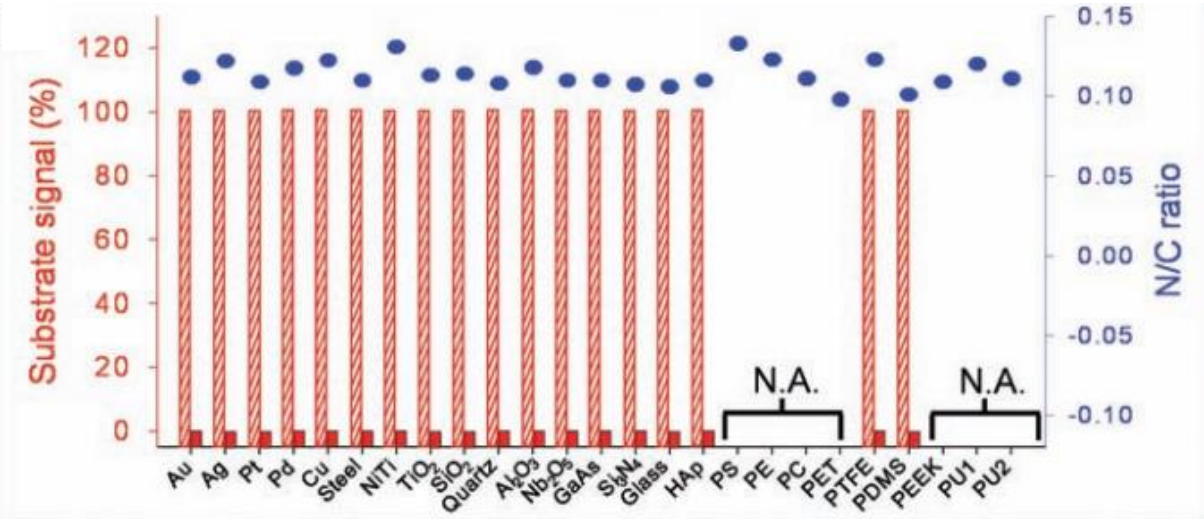

Figure 2.12. XPS characterization of 25 different polydopamine-coated surfaces. The bar graph represents the intensity of characteristic substrate signal before (hatched) and after (solid) coating by polydopamine.

(Haeshin Lee, Shara M. Dellatore, William M. Miller, Phillip B. Messersmith, "Mussel-Inspired Surface Chemistry for Multifunctional Coatings", ***Science***, 318, 5849 (2007). 426-430)

2.2.3.3. Hydrogel based carbon (HBC)

The morphology and its microstructure of HBC were investigated by scanning electron microscopy (SEM). Figure 2.13 shows the inside of the 3D-SGD's surface which can easily pass the water by its capillary channels. Various types of pores ranging from nanometer size to micrometer size have been identified on the SEM and these holes play an important role in pulling water up to capillary forces.

The Brunauer-Emmett-Teller (BET) and adsorption/desorption isotherms were conducted to measure the specific surface area and the Barret-Joyner-Halenda (BJH) method was utilized to measure the porous texture of HBC. Compared with the famous black materials, which are widely used as photo absorbers in solar desalination, we can see that they have an overwhelmingly high surface area. Reduced graphene oxide has 90.597m^2/g, graphite has 1.5622m^2/g, and SWCNT has the 8.192m^2/g surface area, respectively.

To quantitatively analyze the light absorption, the transmittances of HBC were carefully measured also with other famous black materials by a UV-vis-NIR spectrophotometer. Compared to other black materials (rGO: 88%, Graphite: 73%, SWCNT: 91%), HBC showed an overwhelmingly high 97% absorbance, which can be interpreted as having a large effect on vapor generation by absorbing light energy effectively.

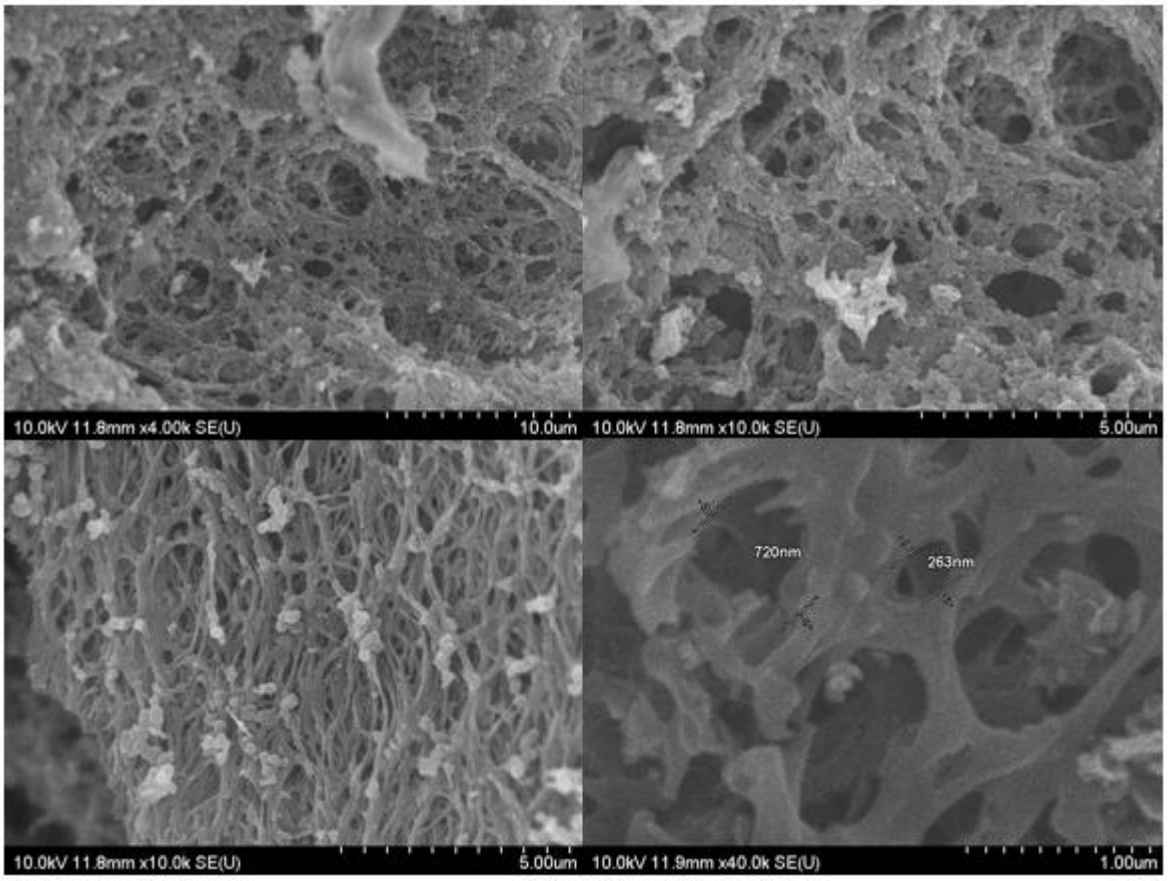

Figure 2.13. SEM images of HBC. Various types of pores ranging from nanometer to micrometer size detected.

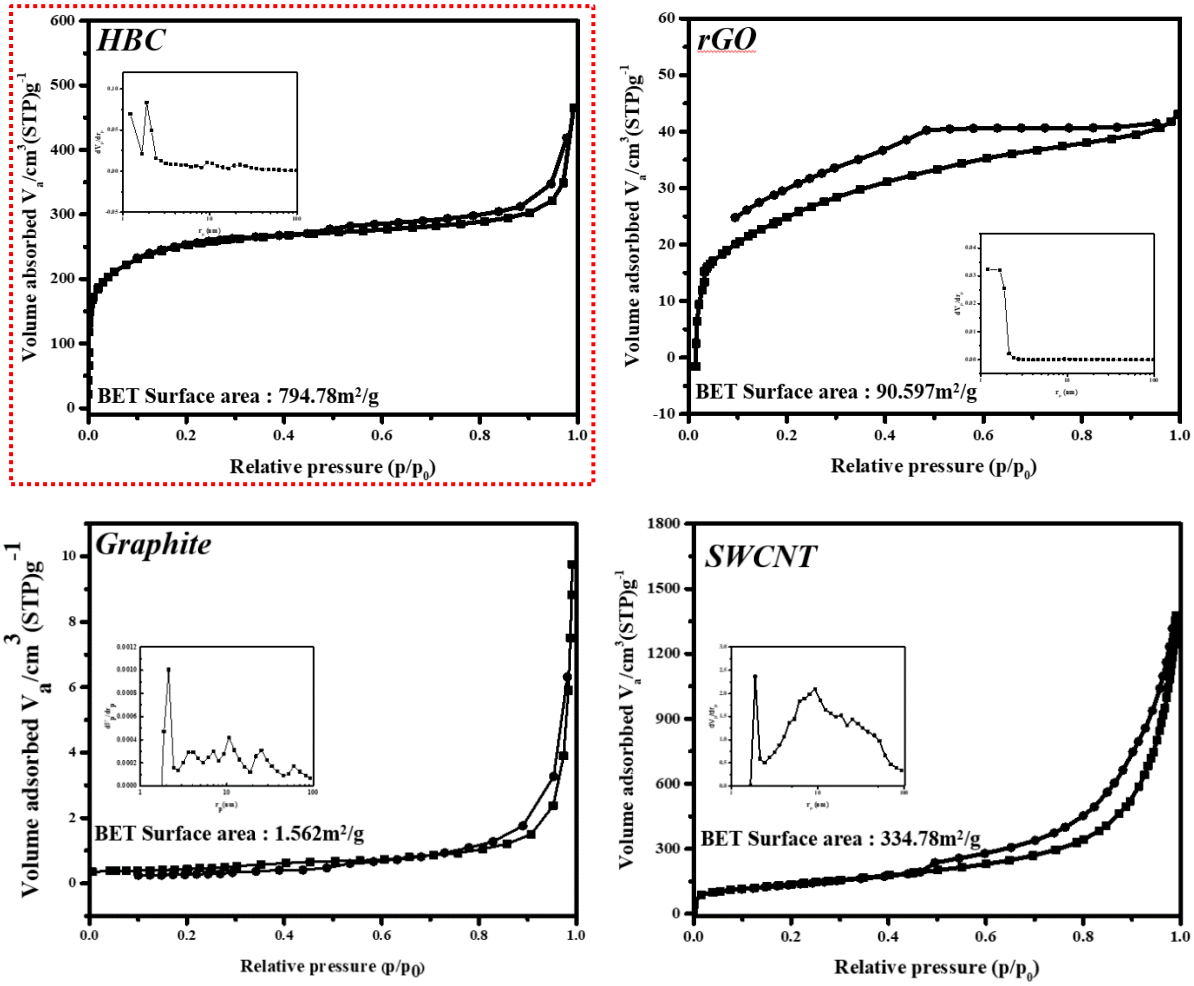

Figure 2.14. BET investigation of the surface area and the pore size distribution of (a) HBC, (b) rGO, (c) Graphite, (d) SWCNT.

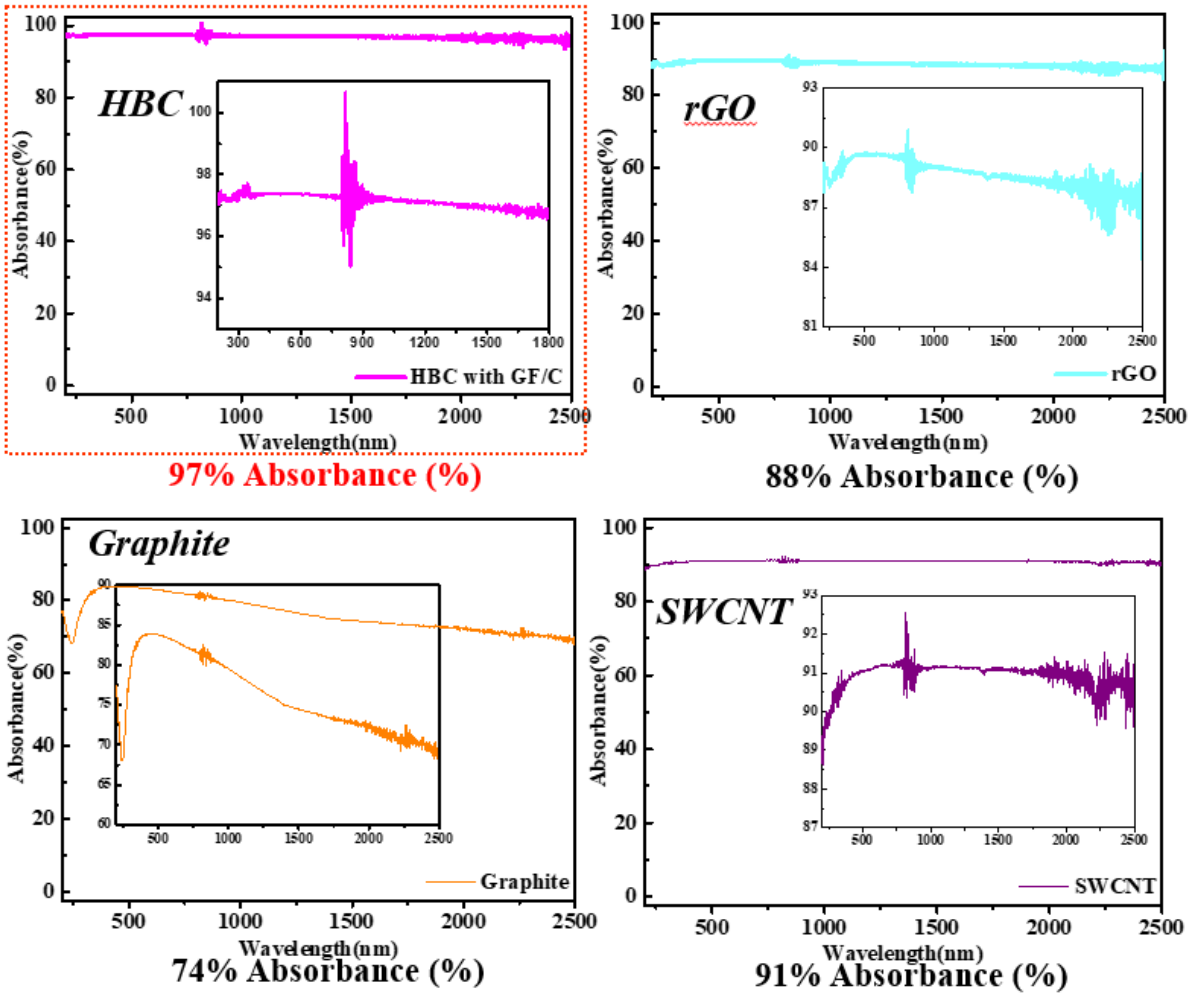

Figure 2.15. Magnified absorption graph for (a) HBC, (b)rGO, (c) Graphite, (d) SWCNT from 300nm to 2500nm wavelength.

2.2.4 Photothermal performance

2.2.4.1. Enhanced performance by 3D printed supporter

We first focus on designing 3D-SGD to maximize the capillary force by finding the narrowest water-path that could be printed with the DLP 3D printer. And then, we build the air pockets inside the sample for self-floating. However, this design lacked the capability to produce relatively high efficiency, and we additionally thought to maximize the area under the sunlight by concave its surface. Light concentration by change its concave design has been realized, but we had to make sure that it showed a similar trend because there is a variable of 3D printed supporter underneath. Along with a reference sample on a flat surface, we had a 20°, 40° slope to change the concavity and double the height of the sample itself to see the difference. We named each 3D printed supporter plane, 20RS (Reentrant surface), 20DRS (double height reentrant surface), 40DRS (double height reentrant surface). The mass change shows that the samples with concave surface treatment appear better performance than the flat plane sample (Figure 2.20). This will be explained based on various aspects of the data.

Light scattering can efficiently occur due to the concave surface, allowing more energy to be confined even with the same light. Figure 2.16 simply shows how light is reflected from the surface of each sample when it is macroscopically exposed to sunlight, and this is supported by the diffuse reflectance shown in figure 2.17. RS substrate combined with HBC has a quite high diffuse reflectance, indicating negligible absorbance. As expected, the larger the degree of curvature, the diffuse reflectance increases. The flat sample shows a sufficiently high diffuse reflectance of about 92%, but the value much more increases approximately to 97% and 98% as the 20RS and 40RS.

Excellent light-harvesting performance is also can confirm by the Infrared thermal camera image. (Figure 2.18). 20RS, 20DRS, 40DRS three samples were taken by FL-IR camera when the solar desalination proceeded under the 1 sun illumination condition. Photographs were taken every 10 minutes, and the range was normalized from 20 to 45 degrees. In these photographs, it is noteworthy that the 20DRS showed the highest insulating effect, and the 40DRS and 20RS decreased gradually. By doubling the z-axis value of the printed supporter, the capillary force does not significantly affect the ability of raise seawater from downside but only can help insulating effect. Figure 2.19 shows the temperature of the surface and the bulk water in 10 minutes interval based on the thermal image of figure 2.18. As mentioned above, since 20DRS has the least amount of heat energy loss to bulk water, it shows the highest surface temperature and the lowest bulk water temperature change at the same time. Interestingly, 20DRS is more effectively blocked heat transfer to the bulk water compared with 40DRS. 40DRS can be more efficient to energy confinement with light scattering (confirmed by figure 2.17), but it is not effective in blocking heat due to the center of the region is too concave and thin. This design also affects the mass change performance aspect. When the 40DRS was immersed in seawater, the middle part of the sample is filled with water due to its large concavity. This causes a surface loss in

which actual evaporation occurs and is directly related to the deterioration of performance.

In sum, we added surface concavity to maximize light scattering to improve performance. However, too large concavity made the opposite effect due to the actual evaporation area's decreasing and the ability as an adiabatic agent deteriorates. So, appropriate concavity where water did not rise to the sample gave the best performance. And by doubling the z-axis value of the sample, we maximize the insulating effect. The sample that reflects all these aspects can output to 20DRS. Furthermore, we added an additional effect to this sample to create 3D-SGD optimized for solar desalination.

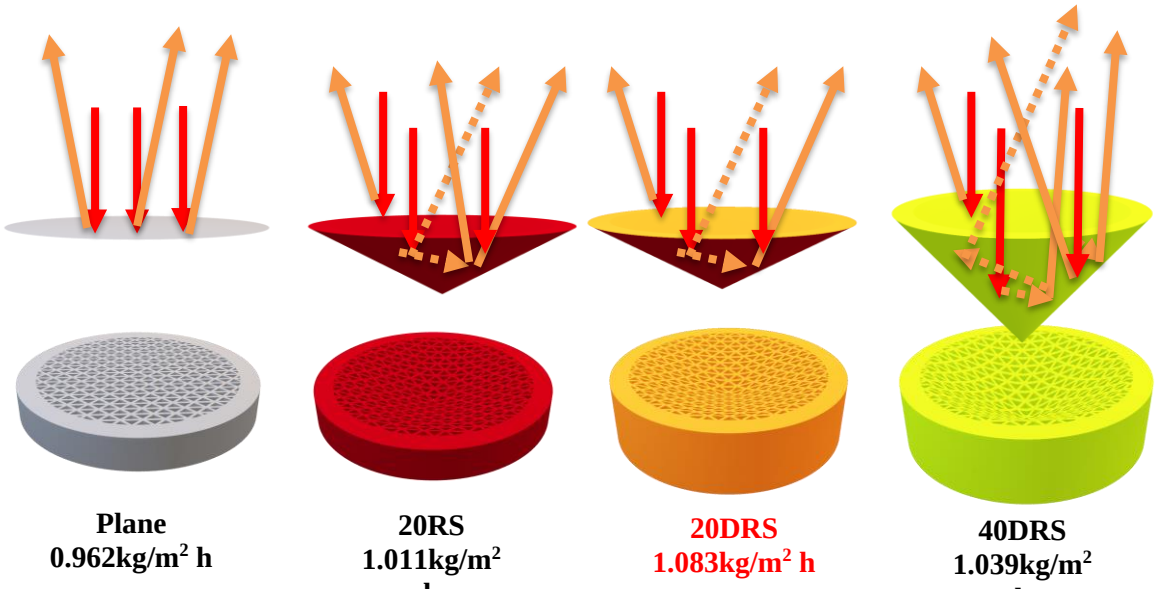

Figure 2.16. 3D printed supporter based on the difference between surface curvature and z-axis value of plane, 20RS, 20DRS, 40DRS. This illustration shows how the light is reflected at the surface of the samples when it receives light.

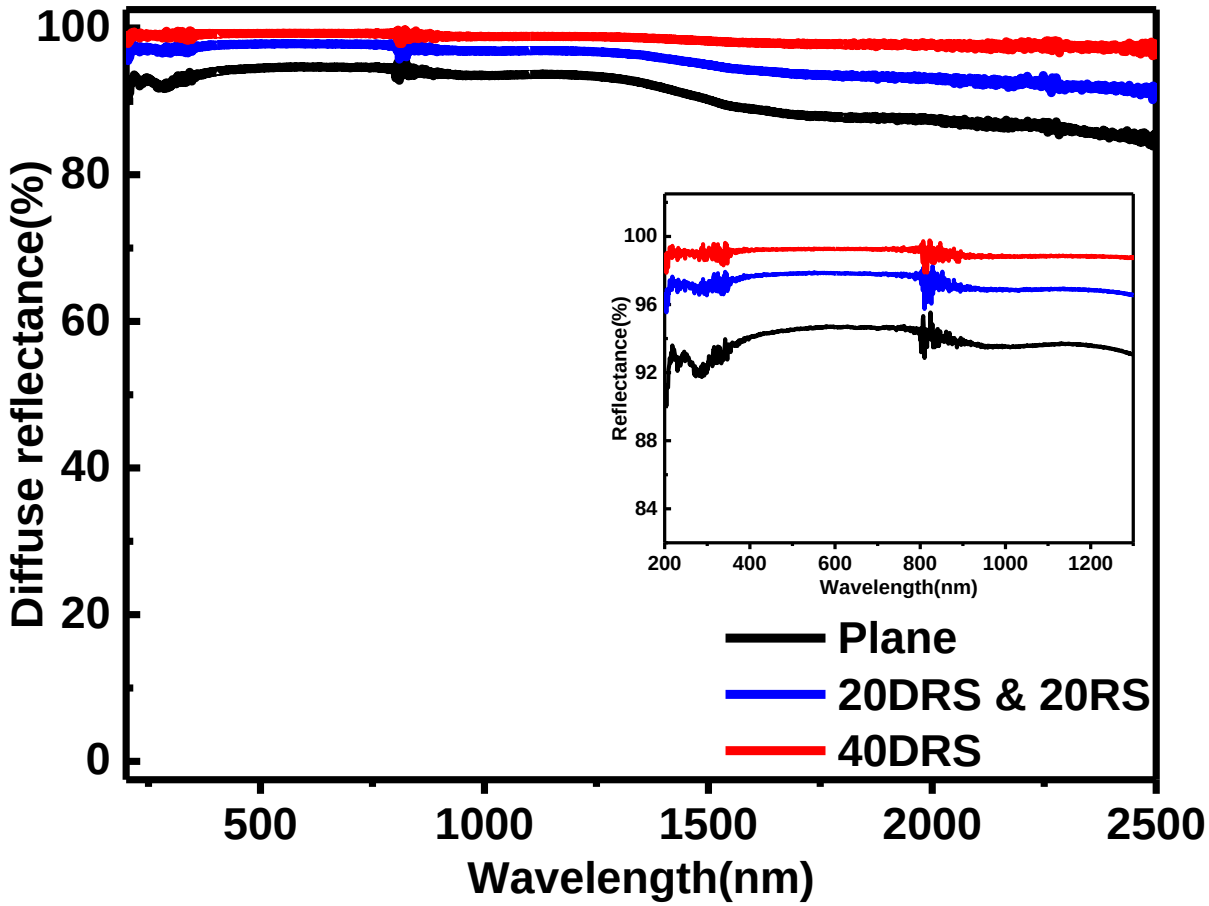

Figure 2.17. Diffuse reflectance of plane, 20RS, 20DRS, and 40DRS.

20DRS

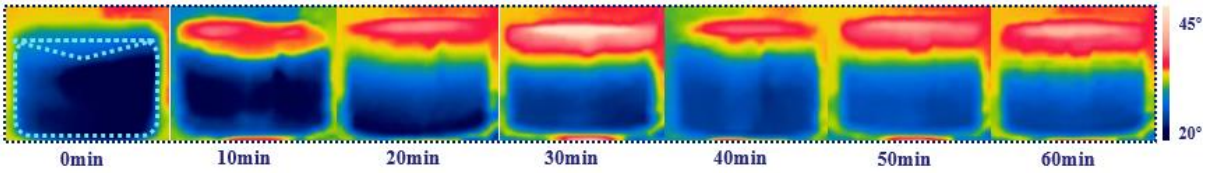

20RS

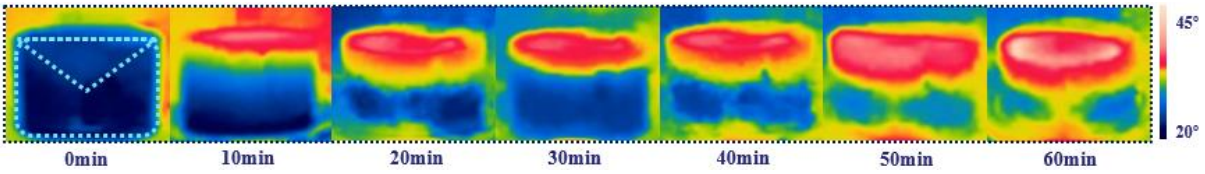

40DRS

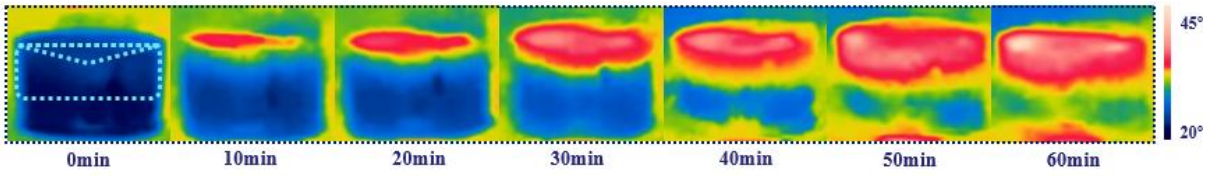

Figure 2.18. Measured thermal conductivity differences by thermal imaging camera (FL-IR).

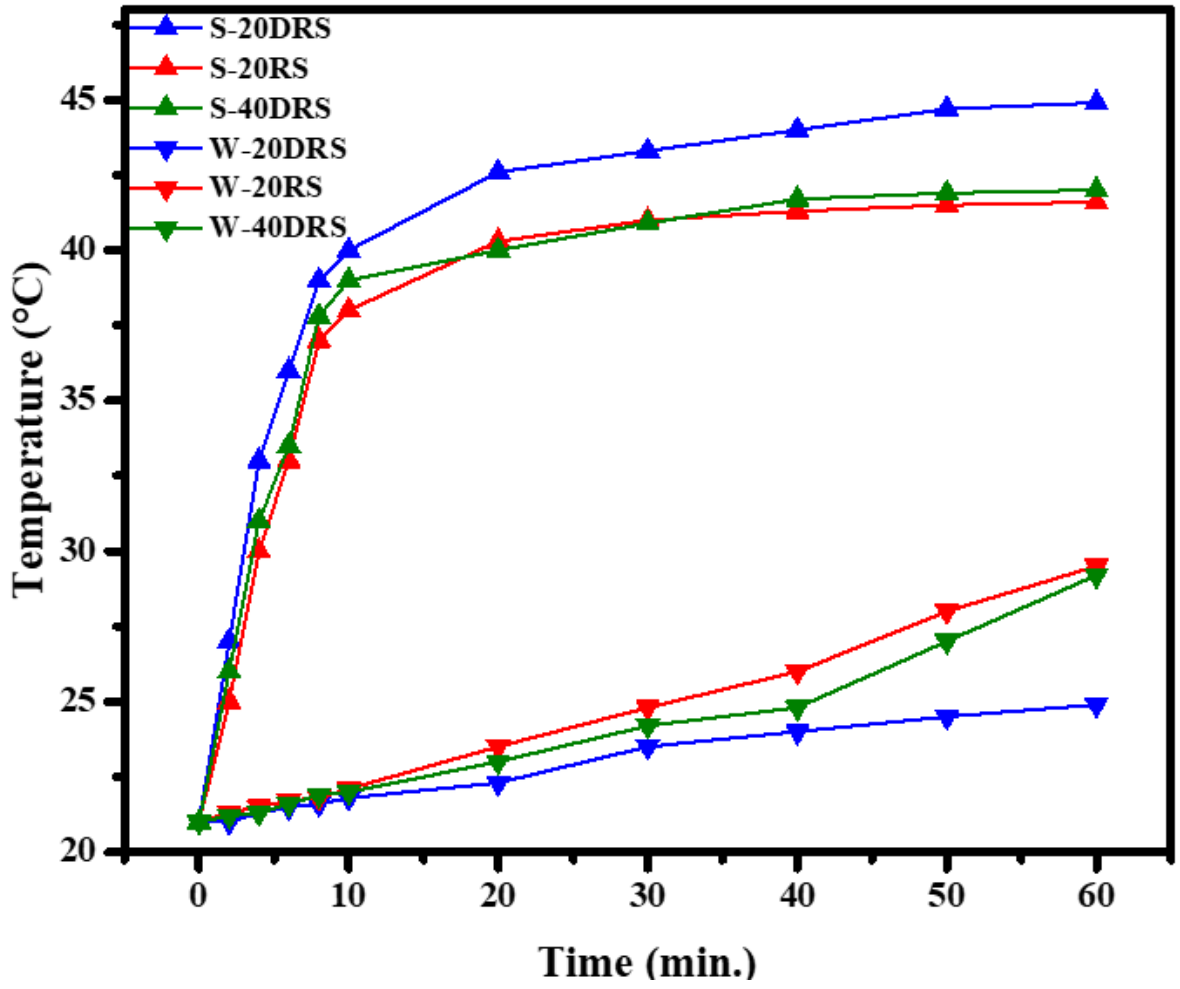

Figure 2.19. Surface temperature and bulk water temperature change by time. 20DRS shows the highest surface temperature and at the same time it acts as a excellent insulator that effectively prevents the heat transfer to bulk water.

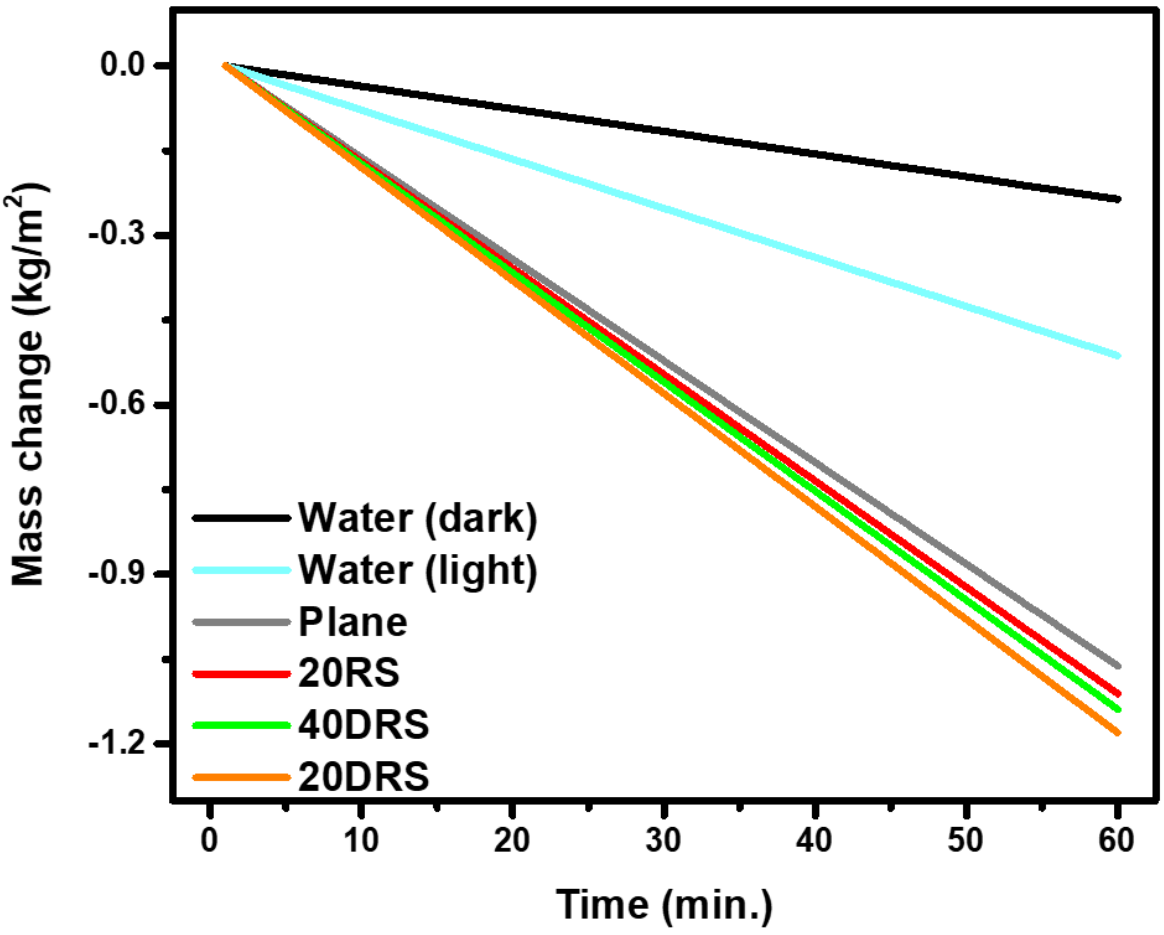

Figure 2.20. Graph showing the water evaporation rate at 1sun for samples with flat surface and curved samples, further divided by the degree of curvature and z-axis value.

2.2.4.2. Enhanced performance by pDA coated GF/C membrane

As mentioned above, a commercial, hydrophilic, and rigid GF/C membrane was not used as such, but it was further treated with polydopamine. The first reason for using pDA was to increase the adhesion through the coating process to attach the carbon material better, and the second reason was to further enhance the steam generation performance by coating hydrophilic dopamine.

Figure 2.21 shows the absorbance of the membrane itself when dipped in a dopamine solution for 4, 8, 12, and 24 hours, respectively, along with pristine GF/C membranes. As we can be expected by shown in a macroscopic view (fig.2.6), it shows the best and the highest level of absorbance when dipped for 24 hours. Figure 2.22 can be fully explained by this evidence. Absorbance (%) was further increased in the dopamine solution for 24 hours than when the HBC is raised on the pristine GF/C membrane. It has been confirmed that it affects the steam generation as well as the adhesion side.

Figure 2.23 shows the difference in adhesion when dopamine coating is applied and not applied to the commercial GF/C membrane. When rubbed by hand, it shows good physical adhesion to pDA coated GF/C, but pristine GF/C didn’t show the same phenomenon. This phenomenon appears more prominently in water (Figure 2.23 (e), (f)). Figure 2.24 shwos the values of storage and loss modulus measured with dma with and without pDA coating treatment. This data also indicates the increase in mechanical strength and adhesion between cth and GF/C membrane.

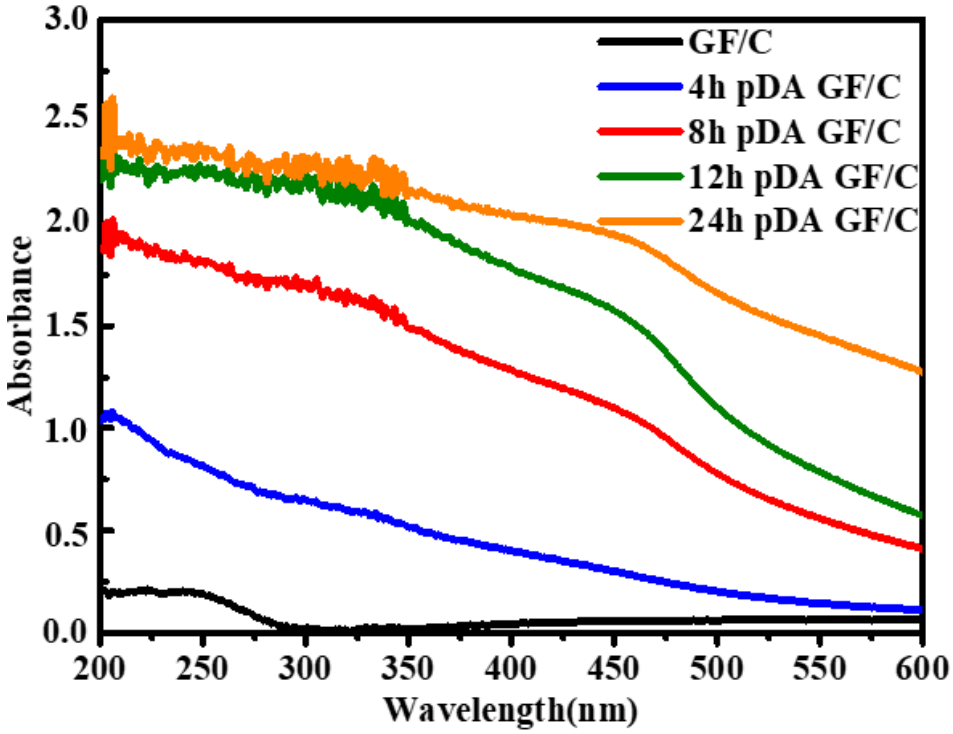

Figure 2.21. Absorbance of pristine GF/C, 2DRS-D4, 2DRS-D8, 2DRS-D12, and 2DRS-D24. Increase dipping time give the better absorbance by itself.

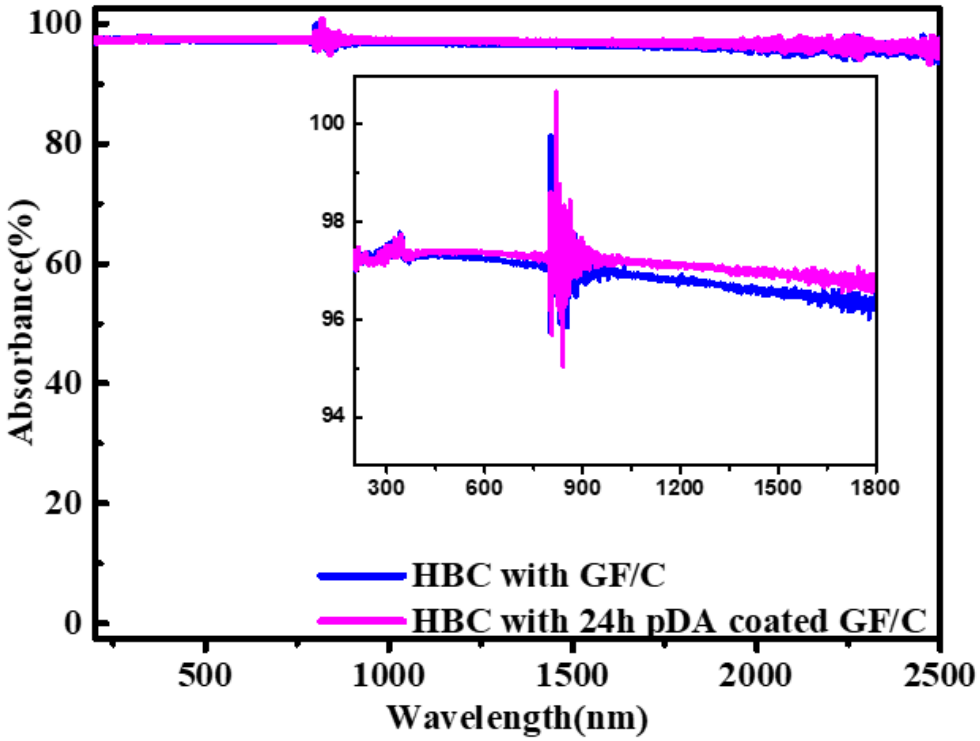

Figure 2.22. Graph shows the difference in absorbance when the HBC is raised on pristine GF/C and when it is on 2DRS-D24.

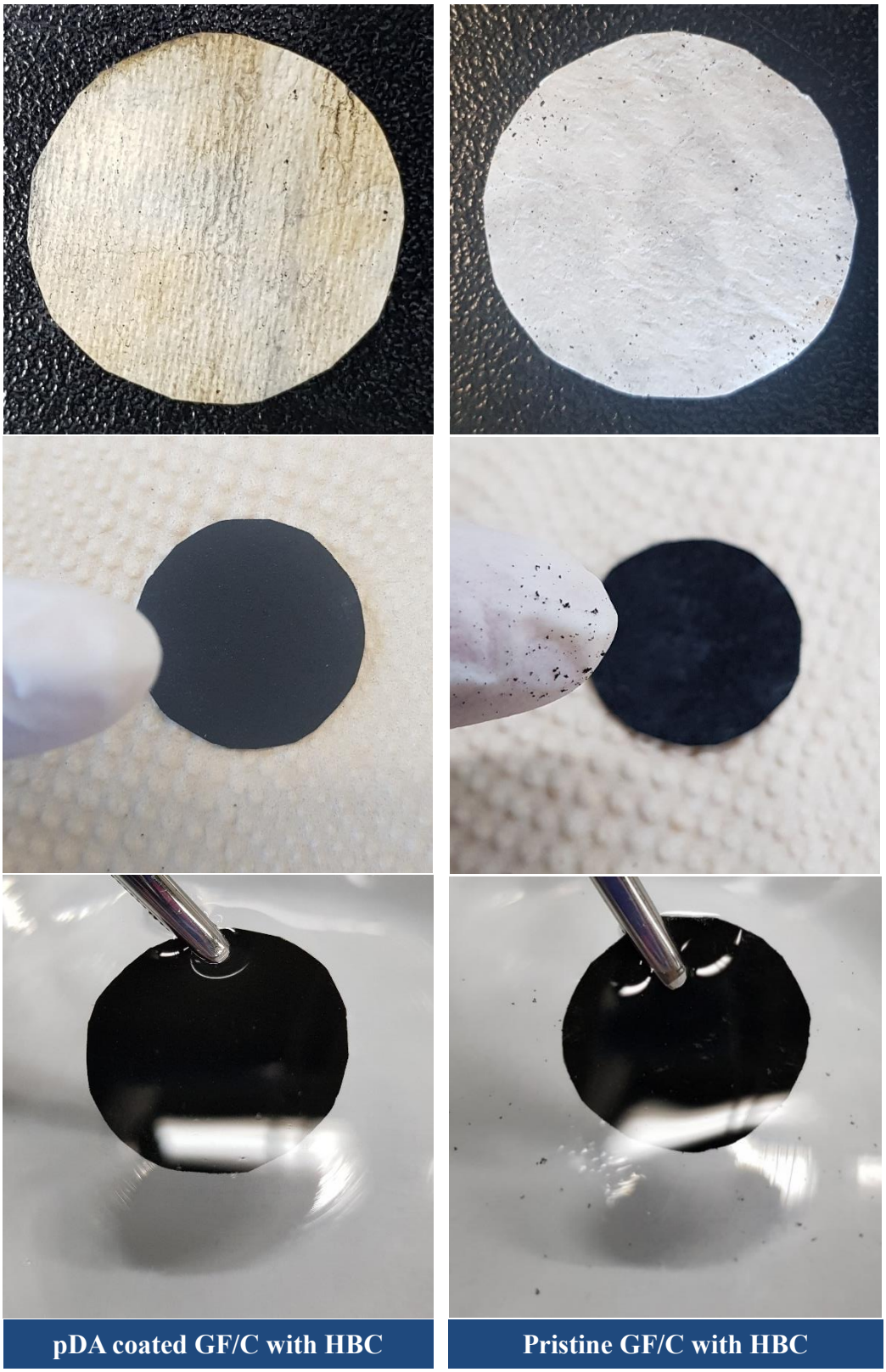

Figure 2.23. Difference in adhesion confirmed by digital camera image. (a), (b) the back of the membranes, (c), (d) images that rubbed the front side of the membrane with HBC, (e), (f) images of each membrane immersed in water.

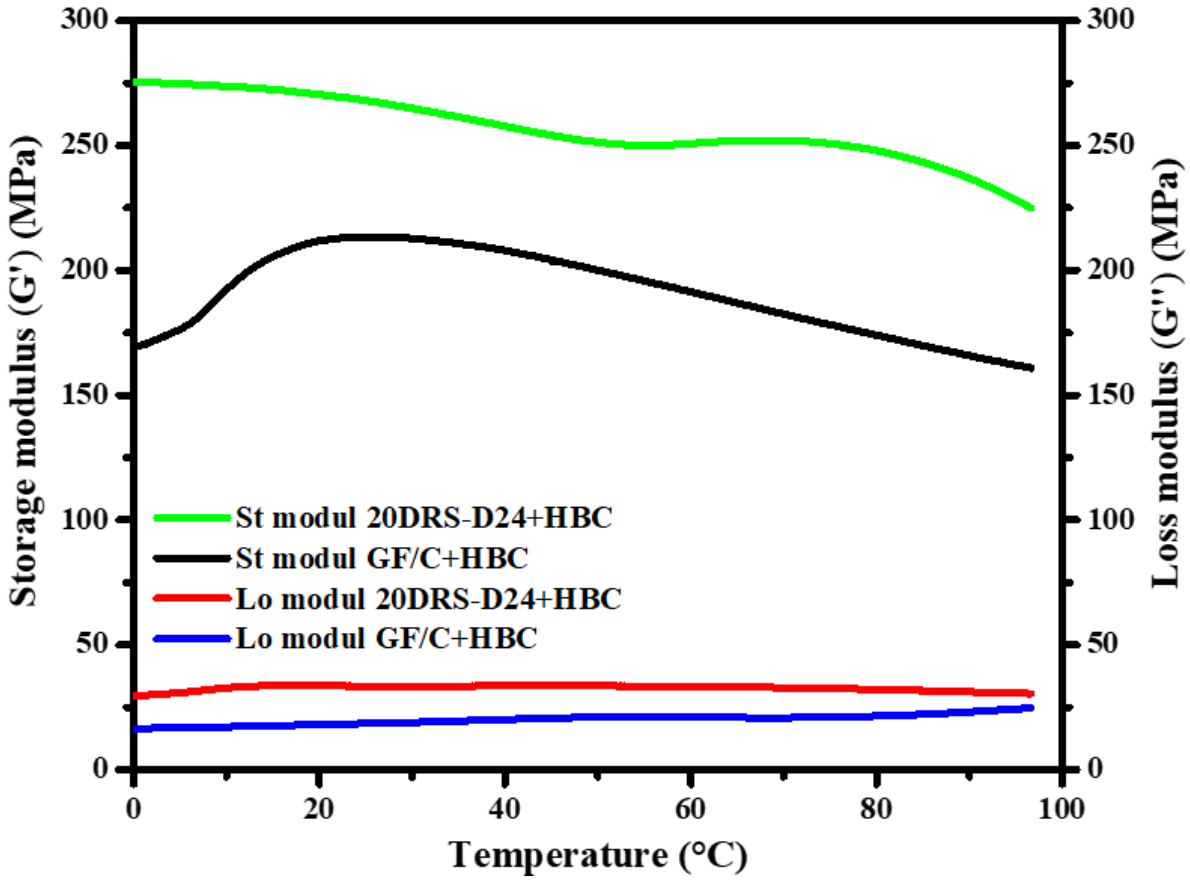

Figure 2.24. The values of storage and loss modulus measured with dma with and without PDA coating treatment.

2.2.4.3. Enhanced performance by HBC

Figure 2.25 shows the hydrophobicity of the HBC by contact angle measurement. To make the membrane as a Janus absorber, the top of the membrane assigned hydrophobicity and the bottom assigned hydrophilicity. It would be slightly reduced the evaporation rate, in contrast, showing extremely good performance on a sustainable aspect. Figure 2.26 shows that the mass change was maintained constantly when a certain amount of water was supplied for 24 hours. Also, it can be confirmed that the evaporation rate was constant even when the device used for desalination is re-measured every hour.

Figure 2.27 shows the zeta potential measurement with other black materials. The filtration of ionic solutes by membranes relies on the charge effect, which performs an important function in the purification performance of porous membranes. Given its negative ζ-potential, the membrane surface possesses ion selectivity. The concentration of counter ions with an opposite sign of charge to the surface ζ-potential of the membrane is higher on the surface of the membrane than in the bulk solution. However, the concentration of the co-ions with the same charge as the surface charge of the membrane is smaller on the membrane surface. A potential difference at the interface, termed the Donnan potential, was created to counteract the transport of counter ions into the HBC layer. Therefore, Na+ ions accumulated on the HBC layer. Figure 2.28 is the schematic of 3D-SGD for zeta potential aspect. High negative zeta potential lead to high osmotic pressure that promote absorption of water from bulk water to top.

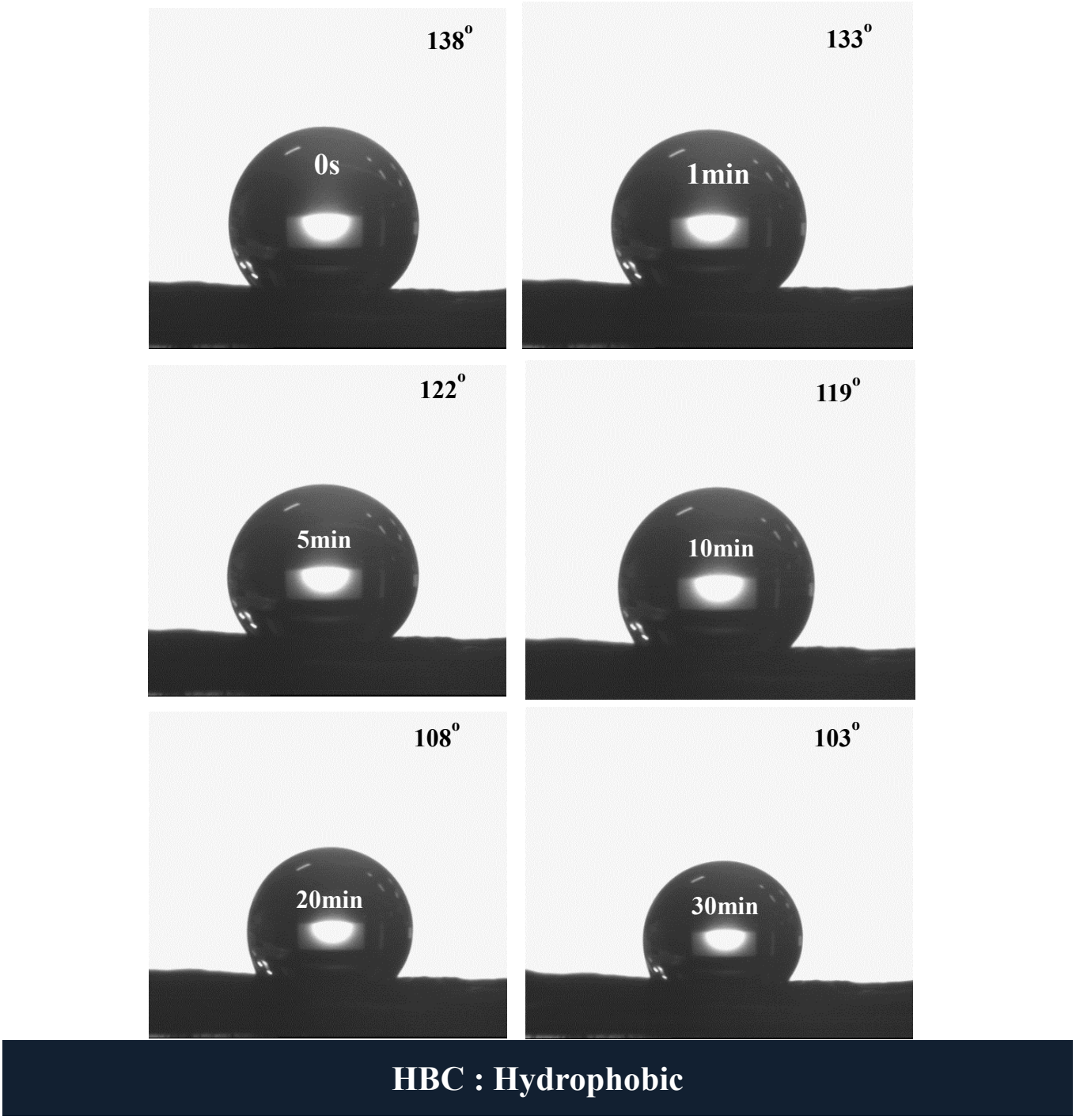

Figure 2.25. Time dependent contact angles of hydrophobic membrane surfaces.

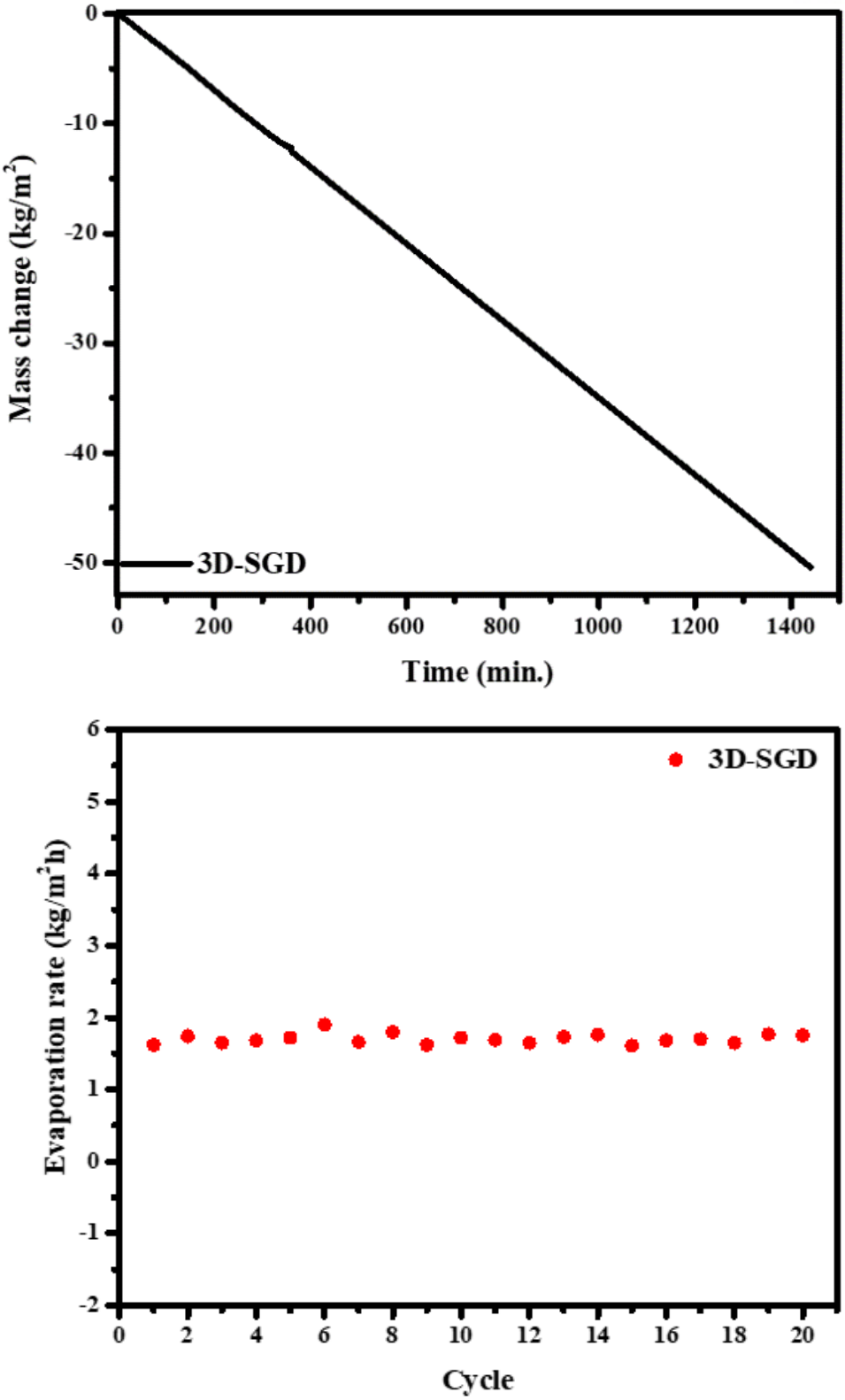

Figure 2.26. (a) Mass change measured for 24 hours. (b) Cycle retention for 20 times.

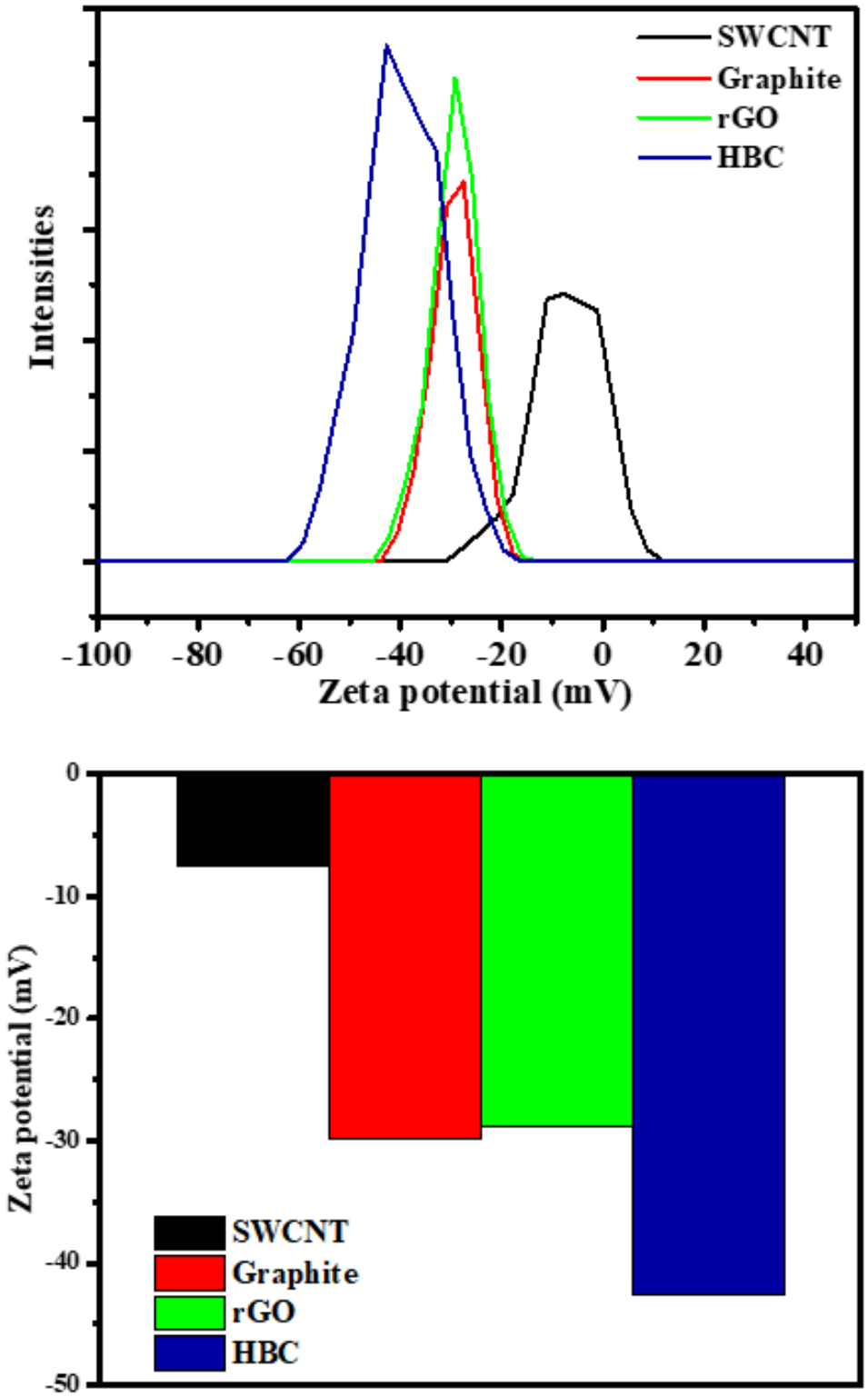

Figure 2.27. Zeta potential of HBC with various black materials (Graphite, rGO, and SWCNT).

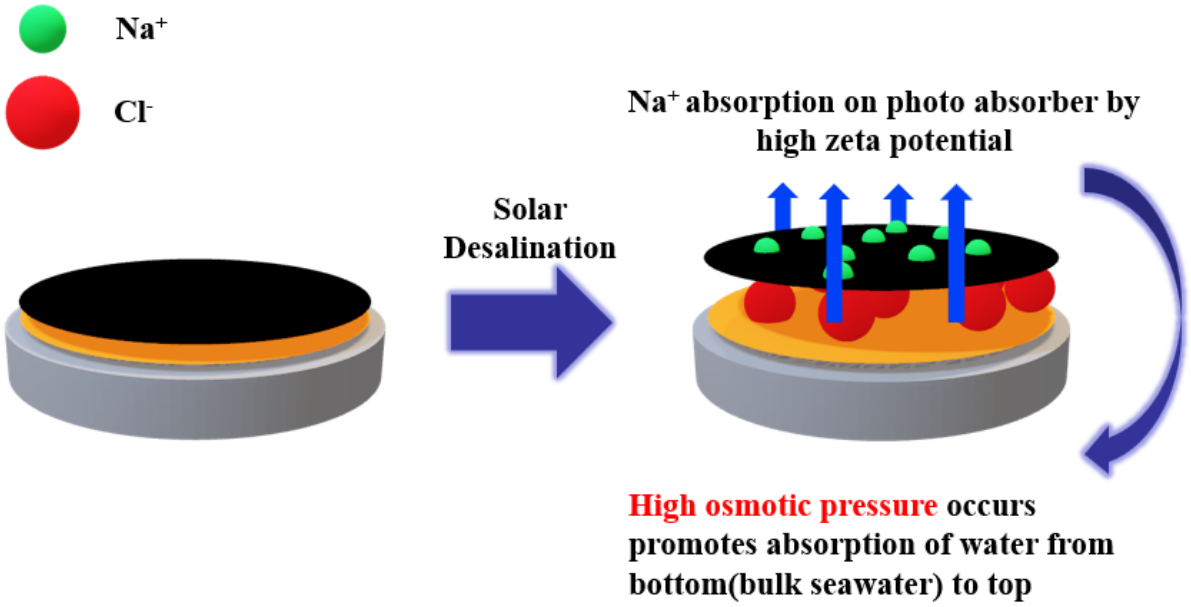

Figure 2.28. Schematic of 3D-SGD for zeta potential aspect. High negative zeta potential lead to high osmotic pressure that promote absorption of water from bulk water to top.

The final mass change is shown in Fig. 2.29 by combining various factors influencing the evaporation rate. As shown in the graph, the final mass change is 1.728kg/m^2, which is close to 90% solar conversion efficiency. The solar thermal efficiency is calculated as,

$$\eta_{th} = \frac{\dot{m} h_{\mathrm{LV}}}{C_{\mathrm{opt}} q_i}$$

η is the solar thermal efficiency, $\dot{m}$ is the mass flux, Copt is the optical concentration, qi is the nominal direct solar irradiation 1Kw/m^2, and h_{LV} is total enthalpy of liquid-vapor phase change (including sensible heat and phase-change enthalpy), can be calculated as,

$$h_{LV} = \lambda + C\Delta T$$

where λ is latent heat of phase change (2260 kJ/kg), C is specific heat capacity of water (4.2 kJ/kg K), and ΔT denotes the temperature increase of the water. Note that the mass flux should be calculated by subtracting the natural evaporation in the dark condition (0.299kg/m^{2}h) from the total evaporation 1.728kg/m^{2}h to realize the real solar conversion efficiency by the solar energy.

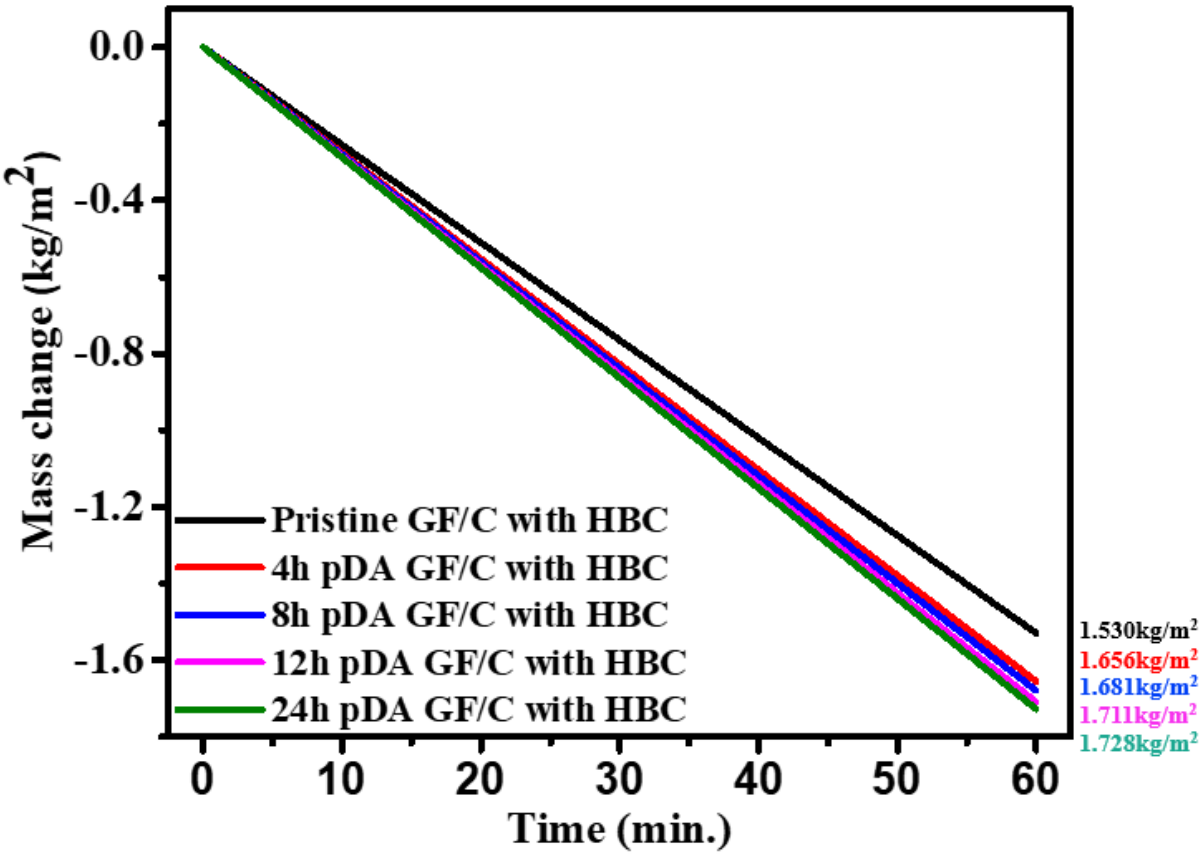

Figure 2.29. Real-time seawater weight loss through the evaporation of the 3D-SGD with different polydopamine dipping time.

2.5 Conclusion

In summary, we used a DLP 3D printer to fabricate a self-floating, insulating, water-path, supporter, and combined with carbon material (HBC) made by carbonization of hydrogel through CVD technique. In addition, the commercial GF/C membrane was used as a prop to raise HBC between 3D printed supporter and HBC. Polydopamine coating treatment was applied to the membrane to increase adhesion and evaporation rate performance. As a result, the completed 3D-SGD sample exhibited high solar absorption (>97%) and Janus characteristics (hydrophobicity/hydrophilicity), resulting in high efficiency in terms of retention at the same. Also, it serves as an effective solar desalination device with an excellent solar-to-vapor conversion efficiency of over 89% under the one sun irradiation (1 kW/m^2). This paper is the first paper to use the sample drawn by the 3d printer in the solar still, showing that the 3d printer which is widely used in various fields can be used for the solar still among the solar desalination. We also expect a solar steam generator capable of solute blocking through a device that continually prevents salt rejection using Janus characteristics.

References

[1] Weichao Xu, Xiaozhen Hu, Shendong Zhuang, Yuxi Wang, Xiuqiang Li, Lin Zhou, Shining Zhu, and Jia Zhu "Flexible and Salt Resistant Janus Absorbers by Electrospinning for Stable and Efficient Solar Desalination", Advanced Energy materials, 2018, 8, 14, 1702884

[2] Zizhao Wang, ‡a Qinxian Ye, ‡a Xingbo Liang, Jiale Xu, Chao Chang, Chengyi Song, Wen Shang, Jianbo Wu, Peng Tao and Tao Deng "Paper-based membranes on silicone floaters for efficient and fast solar-driven interfacial evaporation under one sun", J. Mater. Chem. A, 2017, 5, 16359

[3] Lulu Zhang, Jun Xing, Xinglin Wen, Jianwei Chai, Shijie Wang and Qihua Xiong "Plasmonic heating from indium nanoparticles on a floating microporous membrane for enhanced solar seawater desalination", Nanoscale, 2017, 9, 12843

[4] Zhipeng Liu, Zhenjie Yang, Xichong Huang, Chaoyan Xuan, Jiahui Xie, Huide Fu, Qixing Wu, Junmin Zhang, Xuechang Zhou and Yizhen Liu "High-absorption recyclable photothermal membranes used in a bionic system for high-efficiency solar desalination via enhanced localized heating", J. Mater. Chem. A, 2017, 5, 20044

[5] Xiaofeng Lin, Jiayao Chen, Zhongke Yuan, Meijia Yang, Guojian Chen, Dingshan Yu, Mingqiu Zhang, Wei Hong * and Xudong Chen "Integrative solar absorbers for highly efficient solar steam generation", J. Mater. Chem. A, 2018, 6, 4642

[6] Varun Kashyap, Abdullah Al-Bayati, Seyed Mohammad Sajadi, Peyman Irajizad, Sing Hi Wang and Hadi Ghasemi "A flexible anti-clogging graphite film for scalable solar desalination by heat localization", J. Mater. Chem. A, 2017, 5, 15227

[7] Yuchao Wang, Lianbin Zhang, and Peng Wang "Self-Floating Carbon Nanotube Membrane on Macroporous Silica Substrate for Highly Efficient Solar-Driven Interfacial Water Evaporation", ACS Sustainable Chem. Eng, 2016, 4, 1223-1230

[8] Hadi Ghasemi, George Ni , Amy Marie Marconnet, James Loomis, Selcuk Yerci, Nenad Miljkovic & Gang Chen "Solar steam generation by heat localization ", Nature Communications, 5, 4449

[9] Yiju Li, Tingting Gao, Ahi Yang "Graphene oxide-based evaporator with one-dimensional water transport enabling high-efficiency solar desalination", Nano Energy, 2017, 41, 201-209

[10] Aijun Du*, † Zhonghua Zhu, ‡ and Sean C. Smith "Multifunctional Porous Graphene for Nanoelectronics and Hydrogen Storage: New Properties Revealed by First Principle Calculations", J. AM. Chem. Soc., 2010, 132 (9), 2876-2877

[11] Yanming Liu, Shengtao Yu, Rui Feng, Antoine Bernard, Yang Liu, Yao Zhang, Haoze Duan, Wen Shang, Peng Tao, Chengyi Song, * and Tao Deng "A Bioinspired, Reusable, Paper-Based System for High-Performance Large-Scale Evaporation", Advanced Materials, 2015, 27, 2768-2774

[12] Nathaniel J. Hogan, Alexander S. Urban, Ciceron Ayala-Orozco, Alberto Pimpinelli, Peter Nordlander, and Naomi J. Halas "Nanoparticles Heat through Light Localization", Nano Lett., 2014, 14, 4640-4645

[13] Jianqiu Zhao, Yawei Yang, Chenhui Yang, Yapeng Tian, Yan Han, Jie Liu, Xingtian Yin and Wenxiu Que "A hydrophobic surface enabled salt-blocking 2D Ti3C2 MXene membrane for efficient and stable solar desalination", J. Mater. Chem. A., 2018, 6, 16196-16204

[14] Peihua Yang, Kang Liu, Qian Chen, Jia Li, Jiangjiang Duan, Guobin Xue, Zisheng Xu, Wenke Xie and Jun Zhou "Solar-driven simultaneous steam production and electricity generation from salinity", Energy & Environmental Science, 33, 17276

[15] Kwanghyun Kim, Sunyoung Yu, Cheolwon An, Sung-Wook Kim, and Ji-Hyun Jang, "Mesoporous Three-Dimensional Graphene Networks for Highly Efficient Solar Desalination under 1 sun Illumination", Applied materials & interfaces, 2018, 10, 15602-15608

[16] Xingyi Zhou, Fei Zhao, Youhong Guo, Yi Zhang and Guihua Yu, "A hydrogel-based antifouling solar evaporator for highly efficient water desalination", Energy & Environmental Science, 2018, 11, 1985-1992

[17] Haeshin Lee, Shara M. Dellatore, William M. Miller, and Phillip B. Messersmith "Mussel-Inspired Surface Chemistry for Multifunctional Coatings", Science, 2007, 318, 5849, 426-430

[18] Haeshin Lee, Shara M. Dellatore, William M. Miller, and Phillip B. Messersmith "Femtosecond laser induced robust Ti foam-based evaporator for efficient solar desalination", J. Mater. Chem. A, 2019, 7, 8361-8367

Acknowledgments

아낌없는 조언과 도움을 준 유니스트 SSEL 실험실 구성원 모두와 학부생 때부터 지금까지 저의 지도교수님이셨고, 학교를 벗어나서도 저의 가장 큰 스승님이신 장지현 교수님께 다시 한 번 감사하다는 말씀 전합니다.